Characterization of turbulence in the Mars plasma environment with MAVEN observations

Suranga Ruhunusiri[1], J. S. Halekas[1], J. R. Espley[2], C. Mazelle[3,4], D. Brain[5], Y. Harada[6], G. A. DiBraccio[2], R. Livi[6], D. E. Larson[6], D. L. Mitchell[6], B. M. Jakosky[5], and G. G. Howes[1]

Corresponding author: Suranga Ruhunusiri, Department of Physics and Astronomy, The University of Iowa, Iowa City, Iowa, USA. (suranga-ruhunusiri@uiowa.edu)

[1]Department of Physics and Astronomy, The University of Iowa, Iowa City, Iowa, USA.

[2]NASA Goddard Space Flight Center, Greenbelt, Maryland, USA.

[3]CNRS, IRAP, Toulouse, France.

[4]University Paul Sabatier, Toulouse, France.

[5]Laboratory for Atmospheric and Space Physics, University of Colorado, Boulder, Colorado, USA.

This article has been accepted for publication and undergone full peer review but has not been through the copyediting, typesetting, pagination and proofreading process, which may lead to differences between this version and the Version of Record. Please cite this article as doi: 10.1002/2016JA023456

Abstract.

We characterize turbulence in the Mars plasma environment in a global scale for the first time by computing spectral indices for magnetic field fluctuations (slopes in the magnetic field power spectra) and determining how they vary with frequency and in different regions. In the magnetosheath, unlike in the solar wind, we find an absence of the inertial range which has a spectral index value equal to the Kolmogorov scaling value of $-5/3$. Instead, as observed in the magnetosheaths of other planets, we find that the spectral indices transition from low negative values ~ -0.5 at low frequencies ($<$ proton gyrofrequency) to values much lower than $-5/3$ at high frequencies ($>$ proton gyrofrequency). This indicates that the pristine solar wind is modified at the Martian bow shock and that the fluctuations are dominated by locally generated fluctuations in the magnetosheath. The absence of spectral indices with the Kolmogorov scaling value indicates that the fluctuations in the magnetosheath do not have sufficient time to interact with one another leading to a fully developed energy cascade. Spectral index values near the Kolmogorov scaling value are observed for the low-frequency range near the magnetic pileup boundary and this indicates the presence of fully developed energy cascade. In the wake, we find that the spectral indices

[6]Space Sciences Laboratory, University of California, Berkeley, California, USA.

have approximately the same values, typically ~ -2, for both the low- and high-frequency ranges. We observe seasonal variations of the spectral indices, mainly in the upstream region, which indicate the seasonal variations of the proton cyclotron waves.

1. Introduction

Turbulence arises in fluids and plasmas and this phenomenon refers to the nonlinearly interacting fluctuations that exist in fluids and plasmas. For example, in a fluid, these fluctuations arise in quantities such as the fluid flow velocity while in a magnetized plasma these fluctuations arise in quantities such as the magnetic field and the plasma velocity. The power of these fluctuations P generally has power law relationships with the frequency of the fluctuations f in the form of $P \propto f^{\alpha}$ where α is the spectral index. The spectral indices generally have different values in different frequency ranges and the spectral index value is informative about the physics operating in a certain frequency range such as energy injection, cascade, and dissipation. Investigation of turbulence enables to understand how the energy injected into fluids and plasmas at large spatial or temporal scales is converted to small-scale fluctuations and ultimately to particle heating. Turbulence is also believed to play a prominent role in the heating and acceleration of particles in space plasmas [*Bruno and Carbone*, 2013; *Zimbardo et al.*, 2010].

The solar wind plasma turbulence is the most well-studied turbulence in space plasmas and it has been studied for decades. In the solar wind, the magnetic field power spectrum has distinct spectral breaks that separate the spectrum into four regions, each with a different power law characterized by a unique spectral index [*Tu and Marsch*, 1995; *Bruno and Carbone*, 2013; *Alexandrova*, 2007; *Howes*, 2015; *Kiyani et al.*, 2015]. In particular, for frequencies below 10^{-4} Hz, the spectral index value is ~ -1 and this range of frequencies is referred to as the *energy containing range* [*Matthaeus et al.*, 1994; *Tu and Marsch*, 1995; *Bruno and Carbone*, 2013; *Alexandrova*, 2007]. It is speculated that this range of

frequencies is populated by Alfvén waves that propagate away from the sun. At higher frequencies between 10^{-4} Hz to 0.1 Hz, called the *inertial range*, the spectral index has the Kolmogorov scaling value of -5/3 [*Coleman*, 1968; *Goldstein et al.*, 1995; *Tu and Marsch*, 1995; *Bruno and Carbone*, 2013; *Alexandrova*, 2007]. In this range, in analogy with fluid turbulence, it is interpreted that energy cascade occurs in which the energy is transferred from the lower frequencies to higher frequencies [*Coleman*, 1968; *Goldstein et al.*, 1995; *Tu and Marsch*, 1995; *Bruno and Carbone*, 2013; *Alexandrova*, 2007]. It is believed that this energy cascade occurs in the solar wind via a nonlinear interaction between the counter-propagating Alfvén waves [*Kraichnan et al.*, 1965; *Sridhar and Goldreich*, 1994; *Goldreich and Sridhar*, 1995; *Maron and Goldreich*, 2001]. In the 0.1 Hz to 1 Hz frequency range or the *dissipation range*, the spectral index has a value near -2.8 [*Sahraoui et al.*, 2010; *Roberts et al.*, 2013; *Sahraoui et al.*, 2013; *Roberts et al.*, 2015]. At much higher frequencies, referred to as the *electron-dissipation range*, the spectral index value becomes much lower with a value of ~ -4 [*Sahraoui et al.*, 2009; *Alexandrova et al.*, 2012; *Sahraoui et al.*, 2013; *TenBarge et al.*, 2013]. In these latter two frequency ranges, it is believed that the magnetic energy dissipates into particle heating [*Leamon et al.*, 1998a, b; *Kiyani et al.*, 2009, 2015]. The above-mentioned frequency ranges and the corresponding spectral index values are specified for the solar wind turbulence as measured at ~ 1 AU and the spectral break frequencies change slightly for varying distances from the sun [*Bruno and Carbone*, 2013; *Bourouaine et al.*, 2012; *Bruno and Trenchi*, 2014].

Unlike the solar wind turbulence, turbulence in planetary plasma environments is much less explored. To date turbulence has been characterized for Mercury [*Uritsky et al.*, 2011], Venus [*Vörös et al.*, 2008a, b; *Dwivedi et al.*, 2015], Earth [*Sahraoui et al.*, 2006; *Alexan-*

drova et al., 2008; *Zimbardo et al.*, 2010], Moon [*Luo et al.*, 2016], Jupiter [*Glassmeier*, 1995; *Saur et al.*, 2002; *Tao et al.*, 2015], and Saturn [*Bavassano et al.*, 2000; *von Papen et al.*, 2014; *Hadid et al.*, 2015]. Turbulence in these plasma environments shows both similarities and differences with that of the solar wind turbulence. In particular, similar to the solar wind, magnetic field fluctuations in these plasma environments display different spectral indices in different frequency ranges [*Zimbardo et al.*, 2010; *Hadid et al.*, 2015; *Tao et al.*, 2015]. However, the spectral index in a given frequency range has different values in different regions of a given plasma environment [*Zimbardo et al.*, 2010]. For example, at Earth, low frequency (frequencies less than the proton gyrofrequency) spectral indices have values of -1.0 to -1.7, -1.8, and -1.2 to -1.6, respectively, in the magnetosheath, magnetopause, and the polar cusps [*Zimbardo et al.*, 2010]. Another difference with the solar wind turbulence is the absence of an inertial range with the Kolmogorov scaling spectral index value in some of the planetary plasma environment observations. For example, *Hadid et al.* [2015] observed that, in the magnetosheath of Saturn, the spectral index changes from a value of ~ -1.2 at low frequencies to a value of ~ -2.5 at high frequencies (frequencies higher than the proton gyrofrequency) without forming the intermediate inertial range that has the Kolmogorov scaling value, unlike in the solar wind. The absence of the inertial range has also been observed at the Earth's magnetosheath and Jupiter's magnetosphere [*Zimbardo et al.*, 2010; *Tao et al.*, 2015]. However, the absence of the frequency range with the Kolmogorov scaling value is not a universal feature in planetary plasma environments. For example, the Kolmogorov scaling value is observed for turbulence in the magnetosheath at Earth far downstream from its bow shock, Earth's magnetotail [*Zimbardo et al.*, 2010], Jupiter's magnetosphere [*Glassmeier*,

1995; *Saur et al.*, 2002; *Tao et al.*, 2015], and near the wake region at Venus [*Vörös et al.*, 2008a, b]. For high frequencies, the spectral indices in planetary plasma environments typically have much lower values than in the low-frequency range, analogous to the solar wind turbulence [*Zimbardo et al.*, 2010; *von Papen et al.*, 2014; *Hadid et al.*, 2015; *Tao et al.*, 2015]. However, differences with solar wind turbulence in the high-frequency range have also been observed. For example, at the Earth's magnetosheath, in the electron-dissipation range frequencies, much lower spectral indices, as low as ~ -7.5, have been observed [*Huang et al.*, 2014].

While these characteristics of turbulence in planetary plasma environments have been observed, its interpretation is complicated due to the presence of different characteristic kinetic length scales and timescales in different regions of the planetary plasma environments. The interpretation is further complicated by the fact that the measured plasma fluctuation frequency spectrum in the spacecraft frame consists both the fluctuations in the plasma frame and the spatial structures that are swept by the spacecraft [*Howes et al.*, 2014].

The differences in the solar wind turbulence and turbulence in planetary plasma environments are attributed to the presence of boundaries and instabilities in the planetary plasma environments [*Sahraoui et al.*, 2006; *Yordanova et al.*, 2008; *Sahraoui et al.*, 2004]. The solar wind turbulence develops in a region unimpeded by boundaries such as bow shocks, magnetopause, and ionospheres which are integral features of planetary plasma environments. One consequence of the presence of boundaries such as the bow shock is that the turbulent fluctuations are processed or compressed through the bow shock. If shock-induced instabilities, such as kinetic temperature anisotropy instabilities, gen-

erate new fluctuations, they can dominate over the pre-existing turbulence giving the appearance that the pre-existing fluctuations and their nonlinear relationships have been destroyed. Thus, the turbulence characteristics, for example in the magnetosheath, can be generally different from far upstream of the bow shock which has well-developed energy cascade. These newly generated fluctuations need sufficient time to interact nonlinearly to create an energy cascade. This is believed to be the reason for the presence of the Kolmogorov scaling value in the Earth's magnetosheath far downstream of its bow shock where adequate time is available for the energy cascade to fully develop [*Zimbardo et al.*, 2010].

While a variety of plasma phenomena has been explored at Mars, such as plasma waves and instabilities [*Brain et al.*, 2002; *Espley et al.*, 2004; *Mazelle et al.*, 2004; *Bertucci et al.*, 2005; *Russell et al.*, 2006; *Wei and Russell*, 2006; *Winningham et al.*, 2006; *Gunell et al.*, 2008; *Delva et al.*, 2011; *Wei et al.*, 2011; *Romanelli et al.*, 2013; *Wei et al.*, 2014; *Ruhunusiri et al.*, 2015, 2016a; *Halekas et al.*, 2016; *Ruhunusiri et al.*, 2016b; *Harada et al.*, 2016b; *Romanelli et al.*, 2016], magnetic reconnection [*Eastwood et al.*, 2008; *Halekas et al.*, 2009; *Harada et al.*, 2015], and time dispersed electron and ion events [*Halekas et al.*, 2015; *Harada et al.*, 2016a], plasma turbulence has not been explored in the Martian plasma environment at a global scale. *Gurnett et al.* [2010], using electron density measurements made by the MARSIS instrument in the ionosphere, discovered that within the frequency range 10^{-3} Hz to 10^{-1} Hz, the electron density fluctuations have spectral indices centered at the Kolmogorov scaling value. In this same investigation, using magnetic field values derived from electron cyclotron echoes in a single Mars flyby, *Gurnett et al.* [2010] showed that the magnetic field fluctuations have a Kolmogorov scaling value. In our investigation

of turbulence at Mars, we will perform an extensive characterization of turbulence at the Mars plasm environment encompassing various regions such as upstream of the bow shock, magnetosheath, magnetic pileup region, and the wake region over a wider frequency range, from 5×10^{-3} Hz to 16 Hz. We, in particular, seek to answer the following questions regarding plasma turbulence at Mars:

1. How is the turbulence in the Martian plasma environment similar to and different from the solar wind turbulence?

2. How is the turbulence in the Martian plasma environment similar to and different from the turbulence observed at other planetary plasma environments? For example, are there any similarities and differences for turbulence characteristics between magnetized and unmagnetized planets?

3. Does the turbulence in the Martian plasma environment show any variation to upstream drivers? For example are there any asymmetry in the quasi-parallel and quasi-perpendicular shock regions?

4. Does the turbulence in the Martian plasma environment show any seasonal variations?

2. The Mars plasma environment

Prior to presenting our method and our results, here we briefly review the current state of knowledge regarding the Mars plasma environment for the benefit of the reader. Mars does not have a global intrinsic magnetic field similar to the Earth's dipolar magnetic field [*Acuña*, 1998]. Thus, the solar wind directly interacts with Mars' ionosphere (see Figure 1). This interaction leads to the formation of a bow shock where the supersonic solar wind slows down and diverts around the Mars' ionospheric obstacle [*Sauer et al.*, 1992; *Mazelle*

et al., 2004]. At the subsolar point, the average bow shock distance is $1.5R_M$ where R_M is the radius of Mars [*Mazelle et al.*, 2004; *Trotignon et al.*, 2006]. The region immediately downstream of the bow shock contains thermalized solar wind plasma and this region is called the magnetosheath in analogy with the Earth's magnetosheath [*Mazelle et al.*, 2004]. Further downstream of the bow shock, the magnetic pileup boundary (MPB) forms where the solar wind magnetic field begins to drape and pile up in front of Mars' ionospheric obstacle [*Bertucci et al.*, 2004] and the ion composition begins to be dominated by planetary heavy ions. The region immediately downstream of the MPB is called the magnetic pileup region (MPR) and the magnetic field draping and piling up continues in this region. In the MPR, the composition is dominated by planetary heavy ions. The magnetic field is intensified in the MPR more than in the magnetosheath due to the piling up of the magnetic field. The plasma flow velocity is much lower and the plasma density is much higher in the MPR than in the magnetosheath due to the presence of planetary heavy ions. The wake region is the region downstream of Mars' geometrical shadow and contains Mars' induced magnetotail [*Dubinin et al.*, 1991; *Fedorov et al.*, 2006]. The magnetotail contains planetary escaping ions [*Fedorov et al.*, 2006].

Another important component in the Mars plasma environment is its hydrogen exosphere which extends beyond the bow shock (see Figure 1). The exosphere contains hydrogen atoms which have migrated upward from the Martian atmosphere [*Anderson*, 1974; *Bhattacharyya et al.*, 2015]. Mars' exosphere can extend to an altitude of up to $\sim 9R_M$ [*Bhattacharyya et al.*, 2015]. The exospheric hydrogen atoms are ionized by photoionization, charge exchange, and electron impact ionization resulting from solar extreme ultraviolet (EUV) radiation and solar wind ions and electrons, respectively. This

exospheric ionized component varies seasonally due to the seasonal variation of the EUV flux at Mars arising from the changing distance between Mars and Sun as Mars revolves around the Sun [*Yamauchi et al.*, 2015]. This seasonal variation of the ionized component can in turn cause seasonal variations of the dynamics in the Mars plasma environment.

Our work on turbulence will explore how turbulence evolves in different regions of the Mars plasma environment and determine whether it is influenced by the seasonal variation of Mars' exosphere.

3. Method

We determine the spectral indices for magnetic field fluctuations to characterize turbulence in the Mars plasma environment. For this purpose, we use data from the MAVEN magnetometer (MAG), which is a fluxgate magnetometer that measures vector magnetic fields at 32 samples per second [*Connerney et al.*, 2015a]. The magnetic field data has been corrected for dynamic spacecraft field associated with the solar array operation [*Connerney et al.*, 2015b].

For determination of the spectral indices, first, we start with a time series of the three components of the magnetic field in Mars Solar Orbital (MSO) coordinate system. An example time series for the magnetic field fluctuations observed by MAVEN is shown in Figure 2b. During this time interval, the spacecraft traversed from the magnetic pileup region to the magnetosheath and finally into the upstream region (see Figure 2d). Performing a wavelet transform on the magnetic field time series as in [*Tao et al.*, 2015], we compute power spectral densities (PSDs) for the magnetic field fluctuations (see Figure

2c):

$$PSD(f) = \frac{2\Delta t}{N} \sum_{j=1}^{N} |W_x(t_j, f)|^2 + |W_y(t_j, f)|^2 + |W_z(t_j, f)|^2, \quad (1)$$

where W_x, W_y and W_z are the wavelet transforms of the x, y, and z MSO components of the magnetic field. Here Δt is the inverse sampling rate of the magnetometer. The wavelet transforms are performed using the Morlet wavelet as in [*Tao et al.*, 2015]. To compute PSDs for a long time series, we use 512-second sliding windows that are shifted by 1-minute intervals.

To determine the spectral indices for the magnetic field fluctuations in various regions of the Mars plasma environment, we bin the spatial region traversed by MAVEN from November 2014 to April 2016 into $0.2R_M$ by $0.2R_M$ square grids where R_M is the radius of Mars (see Figure 3a for a MAVEN coverage map). Then in a given bin, we obtain the median PSD for the magnetic field fluctuations. Four examples of such power spectral density spectra, computed in four different regions of the Mars plasma environment, are shown in Figures 3c -3f by red curves. As can be seen in Figure 3, the slope (spectral index) of the PSD for the magnetic field fluctuations below the proton gyrofrequency f_{H+} (shown in blue) is generally different from the slope for the magnetic field fluctuations above f_{H+} (shown in green). In this paper, we will refer to the lower frequency range ($< f_{H+}$) as the MHD range and the higher frequency range ($> f_{H+}$) as the kinetic range. The spectral index histograms for the MHD and the kinetic range for the four different locations shown in Figure 3a are shown in Figure 4 for the interested reader. Comparison of different PSDs in Figure 3 reveals that the spectral indices vary for different locations in the Mars plasma environment. To explore this frequency and spatial variability of the

spectral indices, we plot orbit maps of the spectral indices (see Figure 5). In these maps, the color represents the spectral index value.

Here we note a caveat of using the local f_{H+} for normalizing the frequencies for turbulence characterization at Mars and in planetary plasma environments in general. The fluctuations measured in the spacecraft frame can correspond to Doppler-shifted spatial structures. Thus in some cases, Doppler shifted length scales such as the Taylor shifted gyroradius or the inertial length may turn out to be more appropriate for this normalization. However, the varying plasma flow speeds and other plasma parameters in different magnetospheric regions complicate this determination. Thus, in this work, we use spectra normalized by the local f_{H+} for characterization of turbulence at Mars. The local proton gyrofrequency f_{H+} is suitable for this normalization because visual inspection of magnetic field power spectra reveals that the spectral break generally occurs near the local proton gyrofrequency. Turbulence characterization at other planetary plasma environments has also revealed that the spectral break frequency generally occurs near the local proton gyrofrequency [*Tao et al.*, 2015; *Hadid et al.*, 2015].

When computing the median PSDs shown in Figure 3 and generating our subsequent results (shown in Figures 5-12), we verified that the PSDs used for computing the median lie above the MAG noise level, shown by the black curves in Figures 3c-3f. The MAG noise level was estimated as the minimum PSD value when MAVEN was upstream of the bow shock during the time interval from November 2014 to April 2016. A similar strategy was used by *Tao et al.* [2015] to estimate the Galileo magnetometer noise level. When selecting PSD values from power spectra to compute the median PSD, we only select the

PSD value at a given frequency only if that PSD value is greater than twice the noise level at that frequency.

To determine whether the spectral indices for the magnetic field fluctuations show any seasonal variability, we plot power spectral index maps using observations made at time intervals centered at seasons $Ls \sim 270$, 0, and 90 (see Figures 8a-8c for the MHD range spectral index maps and Figures 8d-8f for kinetic range spectral index maps). These spectral indices were determined using the median PSD spectra for the magnetic field fluctuations computed for each spatial bin for each of the three seasons, similar to the spectra shown in Figure 3. Here Ls refers to the solar longitude and it is 0^0 at the vernal equinox (northern spring), 90^0 at summer solstice, 180^0 at autumnal equinox, and 270^0 at winter solstice. During these times the distance from sun to Mars is approximately 1.56, 1.65, 1.45, and 1.38 AU, respectively. As we discussed in section 2, due to the changes in the distance between Mars and the Sun, the solar EUV flux at Mars varies seasonally and the exospheric density varies accordingly. The idea behind the investigation of the seasonal variation of turbulence is to determine how this exospheric variation influences the turbulence characteristics at Mars. The time intervals that we used for the seasons $Ls \sim 270$, 0, and 90 are, November 27, 2014 to March 17, 2015, June 1, 2015 to October 25, 2015, and Dec 3, 2015 to April 12, 2016, respectively. In addition to being centered on the seasons that are of interest, during these time intervals, MAVEN explored the Mars' upstream region of the bow shock enabling us to also explore how the spectral indices vary as a function of the upstream drivers.

To determine whether the spectral indices show variability in the quasi-parallel and quasi-perpendicular shock regions, we plot spectral index orbit maps using the Mars

Solar Electric (MSE) coordinate system. In the MSE coordinate system, the X axis points toward the sun and it is aligned opposite to the dominant component of the solar wind velocity. The Y axis is aligned with the upstream magnetic field component perpendicular to the X axis and the Z axis is aligned with the upstream convection electric field (see for example Figures 2e and 2f where the MAVEN orbit, corresponding to the time series shown in Figures 2a-2c, is shown in the MSE coordinate system). In the quasi-parallel region we expect enhanced perturbations due to the generation of waves via bow shock reflected solar wind ions and also reflected pickup ions from Mars' extended hydrogen exosphere. The idea behind separating spectral indices into quasi-parallel and quasi-perpendicular regions is to determine the influence of these effects on turbulence in the Mars plasma environment. As can be seen in Figure 7(a), the upstream magnetic field shows a wide range of orientations which means that when MAVEN is in the upstream region it can traverse through these regions enabling us to explore any asymmetries in the quasi-parallel and quasi-perpendicular shock regions (shown in Figures 7(b) and 7(c) respectively). In the MSE coordinate system, the quasi-parallel shock region is located in the $Y_{MSE} > 0$ region when $B_{XMSE} > 0$ (see Figure 7(b)) and in the $Y_{MSE} < 0$ region when $B_{XMSE} < 0$ (see Figure 7(c)) where B_{XMSE} is the X-MSE component of the upstream magnetic field. Quasi-perpendicular shock region, on the other hand, is located in the $Y_{MSE} < 0$ region when $B_{XMSE} > 0$ (see Figure 7(b)) and in the $Y_{MSE} > 0$ region when $B_{XMSE} < 0$ (see Figure 7(c)). To show the spectral index values for the magnetospheric hemisphere containing the quasi-parallel shock region, we plot the spectral index values in a X_{MSE} vs $\sqrt{Y_{MSE}^2 + Z_{MSE}^2}$ orbit map, only including data when $Y_{MSE} > 0$ and $B_{XMSE} > 0$ or $Y_{MSE} < 0$ and $B_{XMSE} < 0$. The MHD range spectral indices are shown in Figures 9a-9c,

while those for the kinetic range are shown in Figures 10a-10c. In these figures, we have plotted separate results for the three seasons of interest. Similarly, to show the spectral index values for the magnetospheric hemisphere containing the quasi-perpendicular shock region, we plot the spectral index values in a X_{MSE} vs $\sqrt{Y_{MSE}^2 + Z_{MSE}^2}$ orbit map only including data when $Y_{MSE} < 0$ and $B_{XMSE} > 0$ or $Y_{MSE} > 0$ and $B_{XMSE} < 0$. The quasi-perpendicular region spectral index values are shown in Figures 9d-9f and Figures 10d- 10f for the MHD and kinetic ranges, respectively.

To determine whether the spectral indices show any asymmetry in the magnetospheric hemispheres in the positive and negative upstream electric field E directions, we use a similar approach to above and plot MSE coordinate system based orbit maps. Here the upstream electric field E refers to the upstream convection electric field given by $E = -V \times B$ where B is the upstream magnetic field and V is the solar wind velocity. Exospheric pickup ion motion is governed by this upstream electric field and as we will discuss in section 5, newly born pickup ions should preferentially excite upstream waves in the positive electric field side. By separating the spectral indices into regions facing the positive and negative electric field sides, we should be able to determine if and how these effects influence evolution of turbulence in the plasma environment of Mars. To show the spectral index values for the magnetospheric hemisphere in the positive electric field direction, we plot them in a X_{MSE} vs $\sqrt{Y_{MSE}^2 + Z_{MSE}^2}$ orbit map only including data when $Z_{MSE} > 0$ since this corresponds to the positive electric field direction in the MSE coordinate system. On the other hand, we plot spectral index values in a X_{MSE} vs $\sqrt{Y_{MSE}^2 + Z_{MSE}^2}$ orbit map only including data when $Z_{MSE} < 0$, to show the spectral index values for the magnetospheric hemisphere in the negative electric field direction.

The spectral index maps for the $E > 0$ region are shown in Figures 11a-11c and Figures 12a-12c for the MHD and kinetic ranges, respectively. Analogously, spectral index maps for the $E < 0$ region are shown in Figures 11d-11f and Figures 12d-12f for the MHD and kinetic ranges, respectively.

4. Results

The spectral indices within both the MHD range and the kinetic range show widely varying values in the Mars plasma environment (see Figure 5). In particular, the MHD range spectral index values decrease when going from near the bow shock to the magnetic pileup region (see Figure 5a). The kinetic range spectral index values, on the other hand, have the opposite trend; the spectral index values increase when going from near the bow shock to the magnetic pileup region (see Figure 5b).

In the MHD range, upstream of the bow shock, the spectral indices are typically -1.2 (see Figure 5a). Near the bow shock and in the magnetosheath, the spectral indices have values close to -0.5. In the magnetic pileup and the wake regions, the spectral indices are much lower in value than in the magnetosheath. In particular, in these regions, the spectral indices typically have values close to -2.0.

The kinetic range spectral indices are generally lower in value than the MHD range spectral indices, except in the magnetic pileup and the wake regions (see Figure 5b). Upstream of the bow shock, the spectral indices in the kinetic range are typically -2.3. Near the bow shock and in the magnetosheath the spectral indices have much lower values with a typical value of -2.7. In the magnetic pileup and the wake regions, the spectral indices are larger than in the magnetosheath. In particular, in these regions, the spectral indices typically have a value of -2.1. One feature to note here is that the spectral indices

in the MHD and the kinetic ranges have approximately equal values in the magnetic pileup region and in the wake. This indicates that, in these regions, within the frequency range that we surveyed, a prominent spectral break is absent. This can also be seen in Figure 3f.

The MHD range spectral indices show seasonal variability (see Figures 8a-8c). This variability is more prominent in the upstream region and in the magnetosheath. In particular, upstream of the bow shock and in the magnetosheath, the spectral index values are much larger for Ls$\sim$ 270 than for Ls$\sim$ 0 and Ls$\sim$ 90 (see Figures 8a-8c). Another interesting trend is that the spectral indices in the night-side magnetosheath are slightly larger for Ls$\sim$ 90 than for Ls$\sim$ 0. In the night-side magnetic pileup region, the spectral indices have generally much lower values for Ls$\sim$ 0 and Ls$\sim$ 90 than for Ls$\sim$ 270. However, this variability is not as prominent as the variability seen in the upstream region and the magnetosheath.

Comparing the orbit maps for the MHD range spectral indices in the magnetospheric hemispheres containing the quasi-parallel and quasi-perpendicular shocks for Ls$\sim$ 270 in Figures 9a and 9d, we find a prominent asymmetry. Specifically, the spectral indices in the upstream region have larger values in the hemisphere containing the quasi-parallel shock. There is no such discernible asymmetry for Ls$\sim$ 0 and Ls$\sim$ 90 (see Figures 9b-9e and Figures 9c-9f).

The spectral indices in the MHD range also show an asymmetry between the E $>$ 0 or E $<$ 0 magnetospheric hemispheres (see Figure 11). This can be prominently seen in the upstream region for Ls$\sim$ 270 (see Figures 11a and 11d). There is no such discernible asymmetry for Ls$\sim$ 0 and Ls$\sim$ 90 (see Figures 11b-11e and Figures 11c-11f).

The kinetic range spectral indices show seasonal variability (see Figures 8d-8f). Upstream of the bow shock, the spectral indices have generally lower values for Ls$\sim$ 270 than for either Ls$\sim$ 0 and Ls$\sim$ 90. This same trend can be seen in the night-side magnetic pileup region. The kinetic range spectral indices also show an asymmetry in the hemispheres containing the quasi-parallel and the quasi-perpendicular shocks (see Figure 10). In particular, for $Ls \sim 270$ the spectral indices in the upstream region have generally much lower values in the quasi-parallel shock region. There is no such discernible asymmetry for $Ls \sim 0$ and $Ls \sim 90$. The spectral index values in the kinetic range do not show any asymmetry between the E > 0 or E < 0 hemispheres (see Figure 12).

5. Discussion

In the solar wind, in the frequency range that correspond to our MHD range, the spectral index value should be typically -5/3 [*Coleman*, 1968; *Goldstein et al.*, 1995; *Tu and Marsch*, 1995; *Bruno and Carbone*, 2013; *Alexandrova*, 2007]. So an interesting question is why our observed upstream spectral index values (as seen in Figure 5) differ from -5/3. As can be seen in Figure 7(a), the upstream magnetic field takes a wide range of orientations with respect to the solar wind flow direction which enables MAVEN to explore quasi-parallel as quasi-perpendicular shock regions when orbiting Mars. The quasi-parallel region can be highly disturbed due to the presence of proton cyclotron waves that can be excited by reflected solar wind protons from the bow shock. Since Mars also has an extended hydrogen exosphere which can give rise to pickup proton populations upstream of Mars, it can also contribute to the generation of upstream proton cyclotron waves (this will be discussed in detail later in this section). The median magnetic field spectra computed in the upstream region contain all these contributing effects. This is

the reason for not observing a spectral index value close to -5/3 in the upstream region for the MHD range frequencies. However, a histogram of the spectral indices in the upstream region should include a relatively large number of spectral indices with values close to -5/3. This can be clearly seen in Figure 4(a). Another way we should be able to identify median spectral index values close to -5/3 in the upstream region is by inspecting upstream region spectral indices for seasons where the exospheric density is lower for example at Ls$\sim$ 0 and Ls$\sim$ 90 (seasons during which the Mars-sun distance is much larger as described in section 3). Inspections of Figure 8(b) and Figure 8(c) for Ls$\sim$ 0 and Ls$\sim$ 90 reveal that in the upstream regions the MHD range spectral indices are in fact much closer to the expected value of -5/3.

The kinetic range spectral indices in the upstream region have values between -2.0 to -3.0 for $Ls \sim 270$ and values between -1.5 to -2.7 for $Ls \sim 0$ and $Ls \sim 90$ (see Figures 8d-8f). In the solar wind, the spectral index in the frequency range that corresponds to our kinetic range is typically -2.8 [*Sahraoui et al.*, 2010; *Roberts et al.*, 2013; *Sahraoui et al.*, 2013; *Roberts et al.*, 2015]. Thus, the kinetic spectral indices in the upstream region at Mars show both similarities and differences to that of the solar wind turbulence. These differences should be a consequence of Mars upstream phenomena which perturb the turbulence characteristics of the pristine solar wind.

Analogous to the observations made at the magnetosheaths of other planets, in the Martian magnetosheath, we find that the spectral indices have low negative values, from -0.4 to -1.0 (see Figure 5a), for the MHD frequency range. This indicates energy injection into the magnetosheath via multiple sources in analogy with interpretations made at other planetary plasma environments [*Vörös et al.*, 2008b]. Spectral indices with similar values

have been observed for the MHD or the low-frequency range at the magnetosheaths of Earth, Jupiter, and Saturn [*Zimbardo et al.*, 2010; *Tao et al.*, 2015; *Hadid et al.*, 2015]. *Vörös et al.* [2008a, b] found similar values for the spectral indices in the Venus magnetosheath in the frequency range 10^{-2} Hz to 0.5 Hz.

For the kinetic range frequencies, similar to the observations made at other planets, we observe that the spectral indices have much lower values than the MHD range spectral indices in the magnetosheath. In particular, we observe values between -2.4 and -2.9 (see Figure 5b). A number of phenomena can lead to the observation of such lower spectral indices which include particle heating, dissipationless cascade [*Boldyrev et al.*, 2012], onset of Landau damping [*Howes et al.*, 2011], undeveloped energy cascade, and weak turbulence [*Sridhar and Goldreich*, 1994; *Galtier*, 2000; *Lithwick and Goldreich*, 2003; *Perez and Boldyrev*, 2008; *Howes et al.*, 2011]. The spectral index value transition in the magnetosheath, from low negative values in the MHD range to high negative values in the kinetic range, without going through a frequency range that has the Kolmogorov scaling value is dissimilar to the spectral index transition in the solar wind. Similar spectral index transitions have been reported for the magnetosheaths of Earth, Jupiter, and Saturn [*Zimbardo et al.*, 2010; *Tao et al.*, 2015; *Hadid et al.*, 2015]. This is indicative of the absence of fully developed energy cascade in the Martian magnetosheath. The kinetic spectral indices with large negative values that we observe are indicative of this undeveloped energy cascade; the spectral index values will be lower than the Kolmogorov scaling value until the fluctuations have time to interact nonlinearly and cascade their energy into smaller scales or in this case higher frequencies. *Hadid et al.* [2015] speculated that while the fully developed energy cascade is absent in the magnetosheath near the

bow shock, it can fully develop farther downstream from the bow shock where sufficient time is available for the fluctuations to interact with one another.

Near the magnetic pileup boundary, the spectral indices in the MHD range have values close to -1.6 (see Figure 5a) or the Kolmogorov scaling value that indicates the presence of fully developed energy cascade in that frequency range. The kinetic range spectral indices, on the other hand, are more negative. Near the magnetic pileup boundary, generation of shear-driven instabilities, such as the Kelvin Helmholtz instability, can be a source of energy injection. If this is indeed the case, the energy injection should occur at frequencies less than $0.1 f_{H+}$, the lower limit of the MHD range because the MHD range has fully developed energy cascade. *Ruhunusiri et al.* [2016b] found partially developed KH vortices with a periodicity of 3 minutes which corresponds to $10^{-2.2}$ Hz or $0.03 f_{H+}$ (assuming $f_{H+} \approx 0.2$ Hz near the MPB). This indicates that the energy injection indeed occurs for frequencies below the MHD range of frequencies. Thus, near the magnetic pileup boundary, the boundary instabilities, such as the KH instability, inject energy that sustains plasm fluctuations. Then the energy cascade occurs followed by particle heating.

Here we note that downstream of the MPB, the spacecraft traversal through boundaries and spatial structures can hinder identification of true turbulence at lower frequencies (typically for frequencies less than $0.1 f_{H+}$ which correspond to ~ 0.02 Hz near the MPB). It is not possible to untangle the spatial and turbulence features using a singe spacecraft. Thus, we do not strictly interpret the lower frequency results in terms of turbulence downstream of the MPB.

In the magnetic pileup and the wake regions, the spectral indices in the MHD and the kinetic ranges both have approximately equal values, ~ -2 and lower (see Figure 5).

Spectral indices values that are lower than -2 have also been observed in the wake region at Venus [*Vörös et al.*, 2008a, b] in a frequency range 10^{-2} Hz to 0.5 Hz. The approximately equal values of the spectral indices in the MHD and the kinetic range implies an absence of the spectral break between those frequency ranges or near the proton gyrofrequency. This can be clearly seen in the PSD shown in Figure 3f. The spectral break tends to occur near the gyrofrequency of the dominant ion species [*von Papen et al.*, 2014]. Since O^+ and O_2^+ are the main ion species in the magnetic pileup and in the wake regions at Mars, the spectral break frequency should occur near $f_{H+}m_{H+}/m_{heavy}$ where m_{H+} is the mass of a proton and m_{heavy} is the mean mass of the ions. If we assume $m_{heavy} = 26m_{H+}$ as in [*Ruhunusiri et al.*, 2016b], the spectral break should occur near $0.04f_{H+}$.

The small positive values of the spectral indices observed in the MHD range for Ls$\sim$ 270 in the upstream region and the magnetosheath (see Figure 8a) indicate the presence of a dominant energy injection mechanism during that time period. The absence of spectral indices with small positive values for Ls$\sim$ 0 and Ls$\sim$ 90 (see Figures 8b and 8c) indicates that this energy injection mechanism is not dominant for these latter time intervals. An investigation of proton cyclotron wave occurrence rate by *Romanelli et al.* [2016], encompassing these same three time periods, revealed a high occurrence rate of proton cyclotron waves at Ls$\sim$ 270 and a drastic diminishment at Ls$\sim$ 0 and Ls$\sim$ 90. Thus, we infer that the small positive values of spectral indices reveal the presence of proton cyclotron waves.

Three sources can be responsible for the generation of these proton cyclotron waves [*Ruhunusiri et al.*, 2016a]: 1. reflected solar wind ions from the bow shock, 2. newly born pickup ions from the exosphere, 3. reflected exospheric pickup ions from the bow

shock. *Halekas et al.* [2016], using the MAVEN observations of periapsis penetrating protons, inferred that the Martian exospheric density should be maximum for Ls$\sim$ 270 and that it shows a decline for Ls$\sim$ 0 and Ls$\sim$ 90. Since the exospheric densities and the proton cyclotron wave occurrence rates are highest at Ls$\sim$ 270 and both of them show diminishments at Ls$\sim$ 0 and Ls$\sim$ 90, we infer that the exospheric ion sources are largely responsible for the generation of the proton cyclotron waves. This result should be intuitively expected because at Ls$\sim$ 270, the distance between Mars and Sun is much smaller than at Ls$\sim$ 0 and Ls$\sim$ 90. Consequently, the solar EUV flux at Mars should be much higher at Ls$\sim$ 270 than at Ls$\sim$ 0 and Ls$\sim$ 90. Since photoionization is a dominant source for ionization of the exospheric Hydrogen at Mars, there should be a large population of pickup ions at Ls$\sim$ 270. These pickup ions, in turn, should lead to the generation of proton cyclotron waves which have a highest occurrence rate at Ls$\sim$ 270.

Closer to Mars, protons are created by photoionization, charge exchange, and electron impact ionization of the neutral hydrogen exosphere. These ions are subsequently accelerated in the upstream solar wind electric field direction and neutralized by charge exchange due to the collisions with the neutral exospheric atoms. These drifting neutrals, which are prominently in the E $>$ 0 region, then undergo ionizations forming newly born pickup ions which excite proton cyclotron waves preferentially in the E $>$ 0 region [*Russell et al.*, 2006]. Thus, if the waves are generated by mechanism 2 mentioned above, they should occur more frequently in the E $>$ 0 hemisphere. However, on the other hand, if the waves are instead generated due to pickup ions that are reflected from the bow shock, this should occur preferentially in the quasi-parallel region because the waves are generated efficiently when the particle populations back stream quasi-parallel to the magnetic field

[*Gary*, 1991]. As can be seen in Figures 11a and 11d, we find that these waves are preferentially generated in the E > 0 hemisphere indicating that the mechanism 2 is efficient at this wave generation. Figures 9a and 9d reveal that the waves are preferentially generated in the quasi-parallel region indicating a preference for mechanism 3 for the generation of the waves. Thus, the asymmetry of the spectral indices in the MHD range between the quasi-parallel and the quasi-perpendicular shock regions (see Figures 9a and 9d) as well as between the E > 0 and the E < 0 regions (see Figures 11a and 11d) that we observe for Ls$\sim$ 270 suggest that the mechanisms 2 and 3 mentioned above should equally contribute to the generation of the proton cyclotron waves.

Similar spectral index asymmetries that we observe between the quasi-parallel and quasi-perpendicular shock regions at Mars in the MHD range have been reported at Earth and Saturn [*Czaykowska et al.*, 2001; *Hadid et al.*, 2015]. In particular, for Earth, *Czaykowska et al.* [2001] reported higher spectral index values for regions downstream of the quasi-parallel bow shock.

We find that the kinetic range spectral indices in the quasi-parallel shock region are lower than in the quasi perpendicular region (see Figures 10a and 10d). Similar trends are reported for the kinetic range spectral indices at Saturn *Hadid et al.* [2015]. However, *Czaykowska et al.* [2001] did not report such a spectral index asymmetry between the regions downstream of the quasi-parallel and the quasi-perpendicular bow shocks at Earth.

6. Conclusions

We characterized turbulence in the Mars plasma environment globally for the first time using the MAVEN magnetometer observations, surveying the frequency range 0.005 Hz to 16 Hz. We computed the spectral indices to characterize turbulence in the Mars plasma

environment and they show a wide range of values in different regions. The MHD range (frequencies less than the proton gyrofrequency) spectral indices are generally higher than the kinetic range (frequencies higher than the proton gyrofrequency) spectral indices.

The turbulence characteristics in the Mars plasma environment show both similarities and differences with the solar wind turbulence. In the MHD range, while a spectral index of -5/3 is expected for the solar wind, we observe values between -0.4 to -1.0 in the magnetosheath, indicating that the turbulence characteristics in the solar wind are modified at the bow shock and that the magnetosheath is dominated by locally generated turbulence. In the magnetosheath, unlike in the solar wind, we find an absence of an intermediate inertial range. Instead, the spectral index values that have low negative values are followed by spectral index values that are much lower than -5/3. The MHD and the kinetic range spectral indices observed at the magnetic pileup boundary are similar to the values that are expected for the pristine solar wind; values close to the Kolmogorov scaling value are observed at the MHD range followed by spectral index values close to -2.8 in the kinetic range. In the magnetic pileup region and in the wake, the MHD and the kinetic range spectral indices have approximately equal values indicating an absence of a spectral break between these two frequency ranges, unlike in the solar wind.

The turbulence characteristics that we observe at Mars are similar to those seen at Venus. The MHD range spectral indices that we observe for the magnetosheath have low negative values as in the magnetosheath at Venus [*Vörös et al.*, 2008a, b]. Near the Venus analog of the magnetic pileup boundary, spectral indices with values near the Kolmogorov scaling value were reported [*Vörös et al.*, 2008a, b]. Similarly, we observe spectral indices with values near the Kolmogorov scaling values for the MHD range frequencies near the

MPB at Mars. In the wake region at Mars, we find spectral indices lower than -2 and the spectral indices observed in the wake region of Venus have exactly the same range of values.

The Martian magnetospheric turbulence characteristics that we observe show similarities with that of the magnetized planets like Earth, Jupiter, and Saturn. The first similarity is the absence of the inertial range with the Kolmogorov scaling value in the magnetosheath. The second similarity is the observation of lower kinetic-range spectral indices in the quasi-parallel bow shock region as reported at Saturn.

We also observe the seasonal variability of spectral indices at Mars. We infer that this indicates the seasonal variability of the proton cyclotron waves. This observed seasonal variability of the spectral indices, together with the asymmetry observed between the quasi-parallel and the quasi-perpendicular regions and the E$>$ 0 and E$<$ 0 regions suggest that the newly born exospheric pickup ions and the bow shock reflected exospheric pickup ions are significant contributors to the generation of proton cyclotron waves.

Acknowledgments. This work was supported by NASA. C. Mazelle was supported by CNES and G. A. DiBraccio was supported by a NASA Postdoctoral Program appointment at the NASA Goddard Space Flight Center, administered by Universities Space Research Association through a contract with NASA. G. Howes was supported by NSF CAREER Award AGS-054061. We thank J. E. P. Connerney for the MAG data. MAVEN data are publicly available through the Planetary Data System.

References

Acuña, M. H., et al. (1998), Magnetic feld and plasma observations at Mars: Initial results from the Mars Global Surveyor Mission, Science, 279, 1676-1680.

Alexandrova, O. (2007), Solar wind vs magnetosheath turbulence and Alfvén vortices, *Nonlin. Processes Geophys.*, *15*, 95-108.

Alexandrova, O., C. Lacombe, and A. Mangeney (2008), Spectra and anisotropy of magnetic fluctuations in the Earth's magnetosheath: Cluster observations, *Ann. Geophys.*, *26*, 3585-3596.

Alexandrova, O., C. Lacombe, A. Mangeney, R. Grappin, and M. Maksimovic (2012), Solar wind turbulent spectrum at plasma kinetic scales, *Astrophys. J.*, *760*, 121, doi:10.1088/0004-637X/760/2/121.

Anderson Jr., D. E. (1974), Mariner 6, 7, and 9 Ultraviolet Spectrometer Experiment: Analysis of hydrogen Lyman alpha data, J. Geophys. Res., 79(10), 15131518, doi:10.1029/JA079i010p01513.

Bavassano Cattaneo, M. B., G. Moreno, G. Russo, and J. D. Richardson (2000), MHD turbulence in Saturn's magnetosheath downstream of a quasi-parallel bow shock, *J. Geophys. Res.*, *105*(A10), 23,141-23,151, doi:10.1029/2000JA000093.

Bertucci, C., C. Mazelle, D. H. Crider, D. L. Mitchell, K. Sauer, M. H. Acua, J. E. P. Connerney, R. P. Lin, N. F. Ness, and D. Winterhalter (2004), MAG/ER observations at the magnetic pileup boundary of Mars: Draping enhancement and low frequency waves, Adv. Space Res., 33, 19381944.

Bertucci, C., C. Mazelle, and M. H. Acuña (2005), Interaction of the solar wind with Mars from Mars Global Surveyor MAG/ER observations, *J. Atmos. Sol. Terr. Phys.*,

67, 1797-1808.

Bhattacharyya, D., J. T. Clarke, J.-L. Bertaux, J.-Y. Chaufray, and M. Mayyasi (2015), A strong seasonal dependence in the Martian hydrogen exosphere, Geophys. Res. Lett., 42, 86788685, doi:10.1002/2015GL065804.

Brain, D. A., F. Bagenal, M. H. Acuña, J. E. P. Connerney, D. H. Crider, C. Mazelle, D. L. Mitchell, and N. F. Ness (2002), Observations of low-frequency electromagnetic plasma waves upstream from the Martian shock, *J. Geophys. Res.*, *107*(A6), doi:10.1029/2000JD000416.

Boldyrev, S., and J. C. Perez (2012), Spectrum of kinetic-Alfvén turbulence, *Astrophys. J. Lett.*, *758*(2), L44.

Bourouaine, S., O. Alexandrova, E. Marsch, and M. Maksimovic (2012), On spectral breaks in the power spectra of magnetic fluctuations in fast solar wind between 0.3 and 0.9 AU, *Astrophys. J.*, *749*, 102.

Bruno, R., and V. Carbone (2013), The solar wind as a turbulence laboratory, *Living Rev. Sol. Phys.*, *10*, 2, doi:10.12942/lrsp-2013-2.

Bruno, R., and L. Trenchi (2014), Radial dependence of the frequency break between fluid and kinetic scales in the solar wind fluctuations, *Astrophys. J. Lett.*, *787*, L24, doi:10.1088/2041-8205/787/2/L24.

Coleman, P. J. Jr. (1968), Turbulence, viscosity, and dissipation in the solar-wind plasma, *Astrophys. J.*, *153*, 371, doi:10.1086/149674.

Connerney, J., J. Espley, P. Lawton, S. Murphy, J. Odom, R. Oliversen, and D. Sheppard (2015a), The MAVEN Magnetic Field Investigation, *Space Sci. Rev.*, 135, doi:10.1007/s11214-015-0169-4.

Connerney, J. E. P., J. R. Espley, G. A. DiBraccio, J. R. Gruesbeck, R. J. Oliversen, D. L. Mitchell, J. Halekas, C. Mazelle, D. Brain, and B. M. Jakosky (2015b), First results of the MAVEN magnetic field investigation, *Geophys. Res. Lett.*, *42*, 88198827, doi:10.1002/2015GL065366.

Czaykowska, A., T. M. Bauer, R. A. Treumann, and W. Baumjohann (2001), Magnetic field fluctuations across the Earth's bow shock, *Annales Geophysicae*, *19*, 275-287.

Delva, M., C. Mazelle, and C. Bertucci (2011), Upstream Ion Cylotron Waves at Venus and Mars, *Space Sci. Rev.*, *162*, 5-24, doi:10.1007/s11214-011-9828-2.

Dubinin, E., R. Lundin, W. Riedler, K. Schwingenschuh, J. G. Luhmann, C. T. Russell, and L. H. Brace (1991), Comparison of observed plasma and magnetic field structures in the wakes of Mars and Venus, J. Geophys. Res., 96(A7), 1118911197, doi:10.1029/91JA01102.

Dwivedi, N. K., D. Schmid, Y. Narita, P. Kovács, Z. Vörös, M. Delva, and T. Zhang (2015), Statistical investigation on the power-law behaviour of magnetic field fluctuations in the Venusian magnetosheath, *Earth Planet Sp.*, *67*, 137.

Espley, J. R., P. A. Cloutier, D. A. Brain, D. H. Crider, and M. H. Acuña (2004), Observations of low-frequency magnetic oscillations in the Martian magnetosheath, magnetic pileup region, and tail, *J. Geophys. Res.*, *109*, A07213, doi:10.1029/2003JA010193.

Eastwood, J. P., D. A. Brain, J. S. Halekas, J. F. Drake, T. D. Phan, M. Øieroset, D. L. Mitchell, R. P. Lin, and M. Acuña (2008), Evidence for collisionless magnetic reconnection at Mars, *Geophys. Res. Lett.*, *35*, L02106, doi:10.1029/2007GL032289.

Fedorov, A., et al. (2006), Structure of the Martian wake, Icarus, 182, 329336, doi:10.1016/j.icarus.2005.09.021.

Galtier, S., S. V. Nazarenko, A. C. Newell, and A. Pouquet (2000), A weak turbulence theory for incompressible MHD, *J. Plasma Phys.*, *63*(5), 447488.

Gary, P. (1991), Electromagnetic ion/ion instabilities and their consequences in space plasmas: a review, *Space Sci. Rev.*, *56*, 373.

Glassmeier, K.-H. (1995), Ultralow frequency pulsations: Earth and Jupiter compared, *Adv. Space Res.*, *16*, 209218.

Goldreich, P., and S. Sridhar (1995), Toward a theory of interstellar turbulence: II. Strong Alfvénic turbulence, *Astrophys. J.*, *438*, 763775, doi:10.1086/175121.

Goldstein, M. L., D. A. Roberts, and W. H. Matthaeus (1995), Magnetohydrodynamic turbulence in the solar wind, *Annu. Rev. Astron. Astrophys.*, *33*, 283326, doi:10.1146/annurev.aa.33.090195.001435.

Gunell, H., *et al.* (2008), Shear driven waves in the induced magnetosphere of Mars, *Plasma Phys. Controlled Fusion*, *50*, 074018.

Gurnett, D. A, D. D. Morgan, F. Duru, F. Akalin, J. D. Winningham, R. A. Frahm, E. Dubinin, and S. Barabash (2010), Large density fluctuations in the Martian ionosphere as observed by the Mars Express radar sounder, *Icarus*, *206*, 83-94.

Hadid, L. Z., F. Sahraoui, K. H. Kiyani, A. Retinó, R. Modolo, P. Canu, A. Masters, and M. K. Dougherty (2015), Nature of the MHD and kintic scale turbulence in the magnetosheath of SATURN: Cassini observartions, *The Astrophys. J. Lett.*, *813*, L29.

Halekas, J. S., J. P. Eastwood, D. A. Brain, T. D. Phan, M. Øieroset, and R. P. Lin (2009), In situ observations of reconnection Hall magnetic fields at Mars: Evidence for ion diffusion region encounters, *J. Geophys. Res.*, *114*, A11204, doi:10.1029/2009JA014544.

Halekas, J. S., *et al.* (2015), Time-dispersed ion signatures observed in the Martian magnetosphere by MAVEN, *Geophys. Res. Lett.*, *42*, 89108916, doi:10.1002/2015GL064781.

Halekas, J. S., *et al.* (2016), Structure, Dynamics, and Seasonal Variability of the Mars-Solar Wind Interaction: MAVEN Solar Wind Ion Analyzer Inflight Performance and Science Results, *J. Geophys. Res.*.

Harada, Y., *et al.* (2015), Magnetic reconnection in the near-Mars magnetotail: MAVEN observations, *Geophys. Res. Lett.*, *42*, 88388845, doi:10.1002/2015GL065004.

Harada, Y., *et al.* (2016a), MAVEN observations of energy-time dispersed electron signatures in Martian crustal magnetic fields, *Geophys. Res. Lett.*, *43*, 939944, doi:10.1002/2015GL067040.

Harada, Y., *et al.* (2016b), MAVEN observations of electron-induced whistler mode waves in the Martian magnetosphere, *J. Geophys. Res.*

Howes, G. G., J. M. TenBarge, and W. Dorland (2011), A weakened cascade model for turbulence in astrophysical plasmas, *Phys. Plasmas*, *18*(10), 102305, doi:10.1063/1.3646400.

Howes, G.G., K.G. Klein, and J.M. TenBarge (2014), Validity of the Taylor hypothesis for linear kinetic waves in the weakly collisional solar wind, *Astrophys. J.*, *789*, 106.

Howes, G. G. (2015), Kinetic turbulence, *Astrophysics*, doi:10.1007/978-3-662-44625-6-6.

Huang, S. Y., F. Sahraoui, X. H. Deng, J. S. He, Z. G. Yuan, M. Zhou, Y. Pang, and H. S. Fu (2014), Kinetic turbulence in the terrestrial magnetosheath: Cluster observations, *Astrophys. J. Lett.*, *789*, L28, doi:10.1088/2041-8205/789/2/L28.

Kiyani, K. H., S. C. Chapman, Yu. V. Khotyaintsev, M. W. Dunlop, and F. Sahraoui (2009), Global Scale-Invariant Dissipation in Collisionless Plasma Turbulence, *Phys.*

Rev. Lett., *103*, 075006.

Kiyani, K. H., K. T. Osman, and S. C. Chapman (2015), Dissipation and heating in solar wind turbulence: from the macro to the micro and back again, *Phil. Trans. R. Soc. A*, *373*, 20140155.

Kraichnan, R. (1965), Inertial range spectrum of hydromagnetic turbulence, *Phys. Fluids*, *8*, 1385.

Leamon, R. J., C. W. Smith, N. F. Ness, W. H. Matthaeus, and H. K. Wong (1998a), Observational constraints on the dynamics of the interplanetary magnetic field dissipation range, J. *Geophys. Res.*, *103*(A3), 47754787, doi:10.1029/97JA03394.

Leamon, R. J., W. H. Matthaeus, C. W. Smith, and H. K. Wong (1998b), Contribution of cyclotron-resonant damping to kinetic dissipation of interplanetary turbulence, *Astrophys. J. Lett.*, *507*, L181.

Lithwick, Y., and P. Goldreich (2003), Imbalanced weak magnetohydrodynamic turbulence, *Astrophys. J.*, *582*, 1220, doi:10.1086/344676.

Luo, Q. Y., L. Yang, and J. H. Ji (2016), Global distribution of the kinetic scale magnetic turbulence around the moon, *Astrophys. J. Lett.*, *816*, L3.

Maron, J., and P. Goldreich (2001), Simulations of incompressible magnetohydrodynamic turbulence, *Astrophys. J.*, *554*, 11751196, doi:10.1086/321413.

Matthaeus, W. H., S. Oughton, D. H. Pontius Jr., and Y. Zhou (1994), Evolution of energy-containing turbulent eddies in the solar wind, *J. Geophys. Res.*, *99*(A10), 1926719287, doi:10.1029/94JA01233.

Mazelle, C., *et al.* (2004), Bow Shock and Upstream phenomena at Mars, *Space Sci. Rev.*, *111*, 115181.

Perez, J. C. and S. Boldyrev (2008), On Weak and Strong Magnetohydrodynamic Turbulence, *Astrophys. J. Lett.*, *672*, L61.

Roberts, O. W., X. Li, and B. Li (2013), Kinetic plasma turbulence in the fast solar wind measured by Cluster, *Astrophys. J.*, *769*, 58, doi:10.1088/0004-637X/769/1/58.

Roberts, O. W., X. Li, and L. Jeska (2015), A statistical study of the solar wind turbulence at ion kinetic scales using the k-filtering technique and Cluster data, *Astrophys. J.*, *802*, 2, doi:10.1088/0004-637X/802/1/2.

Romanelli, N., C. Bertucci, D. Gómez, C. Mazelle, and M. Delva (2013), Proton cyclotron waves upstream from Mars: Observations from Mars Global Surveyor, *Planet. Space Sci.*, *76*, 1-9.

Romanelli, N., *et al.* (2016), Proton cyclotron waves occurrence rate upstream from Mars observed by MAVEN: associated dynamics of the Martian upper atmosphere, *J. Geophys. Res.*

Ruhunusiri, S., J. S. Halekas, J. E. P. Connerney, J. R. Espley, J. P. McFadden, D. E. Larson, D. L. Mitchell, C. Mazelle, and B. M. Jakosky (2015), Low-frequency waves in the Martian magnetosphere and their response to upstream solar wind driving conditions, *Geophys. Res. Lett.*, *42*, 89178924, doi:10.1002/2015GL064968.

Ruhunusiri, S., *et al.* (2016a), MAVEN observation of an obliquely propagating low-frequency wave upstream of Mars, *J. Geophys. Res. Space Physics*, *121*, 23742389, doi:10.1002/2015JA022306.

Ruhunusiri, S., *et al.* (2016b), MAVEN observations of partially developed Kelvin-Helmholtz vortices at Mars, *Geophys. Res. Lett.*, *43*, 47634773, doi:10.1002/2016GL068926.doi:10.1002/2015GL064968.

Russell, C. T., S. S. Mayerberger, and X. Blanco-Cano (2006), Proton cyclotron waves at Mars and Venus, *Adv. Space Res.*, *38*, 745-751.

Sahraoui, F., G. Belmont, J. L. Pinon, L. Rezeau, A. Balogh, P. Robert, and N. Cornilleau-Wehrlin (2004), Magnetic turbulent spectra in the magnetosheath: New insights, *Ann. Geophys.*, *22*, 22832288.

Sahraoui, F., G. Belmont, L. Rezeau, N. Cornilleau-Wehrlin, J. Pinon, and A. Balogh (2006), Anisotropic turbulent spectra in the terrestrial magnetosheath as seen by the Cluster spacecraft, *Phys. Rev. Lett.*, *96*(7), 075,002, doi:10.1103/PhysRevLett.96.075002.

Sahraoui, F. M. L. Goldstein, P. Robert, and Yu. V. Khotyaintsev (2009), Evidence of a Cascade and Dissipation of Solar-Wind Turbulence at the Electron Gyroscale, *Phys. Rev. Lett.*, *102*, 231102.

Sahraoui, F., M. L. Goldstein, G. Belmont, P. Canu, and L. Rezeau (2010), Three dimensional anisotropic k spectra of turbulence at subproton scales in the solar wind, *Phys. Rev. Lett.*, *105*, 131101.

Sahraoui, F., S. Y. Huang, G. Belmont, M. L. Goldstein, A. Retinó, P. Robert, and J. de Patoul (2013), Scaling of the electron dissipation range of solar wind turbulence, *Astrophys. J.*, *777*, 15, doi:10.1088/0004-637X/777/1/15.

Sauer, K., T. Roatsch, U. Motschmann, K. Schwingenschuh, R. Lundin, H. Rosenbauer, and S. Livi (1992), Observations of plasma boundaries and phenomena around Mars with Phobos 2, J. Geophys. Res., 97(A5), 62276233, doi:10.1029/91JA02972.

Saur, J., H. Politano, A. Pouquet, and W. Matthaeus (2002), Evidence for weak MHD turbulence in the middle magnetosphere of Jupiter, *Astron. Astrophys.*, *386*, 699.

Sridhar, S., and P. Goldreich (1994), Towards a theory of interstellar turbulence: I. Weak Alfvénic turbulence, *Astrophys. J.*, *432*, 612621.

Tao, C., F. Sahraoui, D. Fontaine, J.de Patoul, T. Chust, S. Kasahara, and A. Retinó (2015), Properties of Jupiter's magnetospheric turbulence observed by the Galileo spacecraft. *J. Geophys. Res. Space Physics*, *120*, 24772493, doi: 10.1002/2014JA020749.

TenBarge, J. M., G. G. Howes, and W. Dorland (2013), Collisionless damping at electron scales in solar wind turbulence, *Astrophys. J.*, *774*, 139.

Trotignon, J., C. Mazelle, C. Bertucci, and M. Acuña (2006), Martian shock and magnetic pile-up boundary positions and shapes determined from the phobos 2 and mars global surveyor data sets, *Planet. Space Sci.*, *54*(4), 357 369, doi:10.1016/j.pss.2006.01.003.

Tu, C.-Y., and E. Marsch (1995), MHD structures, waves and turbulence in the solar wind: Observations and theories, *Space Sci. Rev.*, *73*, 1210, doi:10.1007/BF00748891.

Uritsky, V. M., J. A. Slavin, G. V. Khazanov, E. F. Donovan, S. A. Boardsen, B. J. Anderson, and H. Korth (2011), Kinetic-scale magnetic turbulence and finite Larmor radius effects at Mercury, *J. Geophys. Res.*, *116*, A09236, doi:10.1029/2011JA016744.

von Papen, M., J. Saur, and O. Alexandrova (2014), Turbulent magnetic field fluctuations in Saturn's magnetosphere, *J. Geophys. Res. Space Physics*, *119*, 27972818, doi:10.1002/2013JA019542.

Vörös, Z., T. L. Zhang, M. P. Leubner, M. Volwerk, M. Delva, W. Baumjohann, and K. Kudela (2008a), Magnetic fluctuations and turbulence in the Venus magnetosheath and wake, *Geophys. Res. Lett.*, *35*, L11102, doi:10.1029/2008GL033879.

Vörös, Z., T. L. Zhang, M. P. Leaner, M. Volwerk, M. Delva, and W. Baumjohann (2008b), Intermittent turbulence, noisy fluctuations, and wavy structures in the Venusian mag-

netosheath and wake, *J. Geophys. Res.*, *113*, E00B21, doi:10.1029/2008JE003159.

Winningham, J. D., *et al.* (2006), Electron oscillations in the induced Martian magnetosphere, *Icarus*, *182*, 360370.

Wei, H. Y., and C. T. Russell (2006), Proton cyclotron waves at Mars: Exosphere structure and evidence for a fast neutral disk, *Geophys. Res. Lett.*, *33*, L23103, doi:10.1029/2006GL026244.

Wei, H. Y., C. T. Russell, T. L. Zhang, and X. Blanco-Cano (2011), Comparative study of ion cyclotron waves at Mars, Venus and Earth, *Planet. Space Sci.*, *59*, 1039-1047.

Wei, H. Y., M. M. Cowee, C. T. Russell, and H. K. Leinweber (2014), Ion cyclotron waves at Mars: Occurrence and wave properties, *J. Geophys. Res. Space Physics*, *119*, 52445258, doi:10.1002/2014JA020067.

Yamauchi, M., *et al.* (2015), Seasonal variation of Martian pick-up ions: Evidence of breathing exosphere, *Planet. Space Sci.*, *119*, 54-61.

Yordanova, E., A. Vaivads, M. André, S. C. Buchert, and Z. Vörös (2008), Magnetosheath plasma turbulence and its spatiotemporal evolution as observed by the cluster spacecraft, *Phys. Rev. Lett.*, *100*(20), 205003.

Zimbardo, G., A. Greco, L. Sorriso-Valvo, S. Perri, Z. Vörös, G. Aburjania, K. Chargazia, and O. Alexandrova (2010), Magnetic turbulence in the geospace environment, *Space Sci. Rev.*, *156*, 89-134.

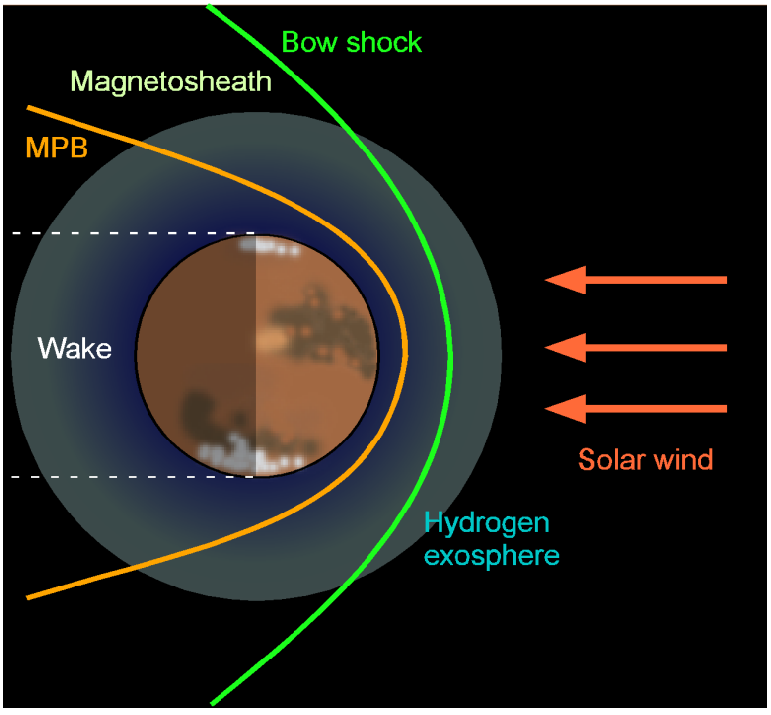

Figure 1. (a) The Mars plasma environment. The bow shock separates the upstream solar wind from the magnetosheath. The magnetic pileup boundary separates the magnetosheath from the magnetic pileup region. The hydrogen exosphere, which extends beyond the bow shock of Mars, is also a crucial component in the Mars plasma environment.

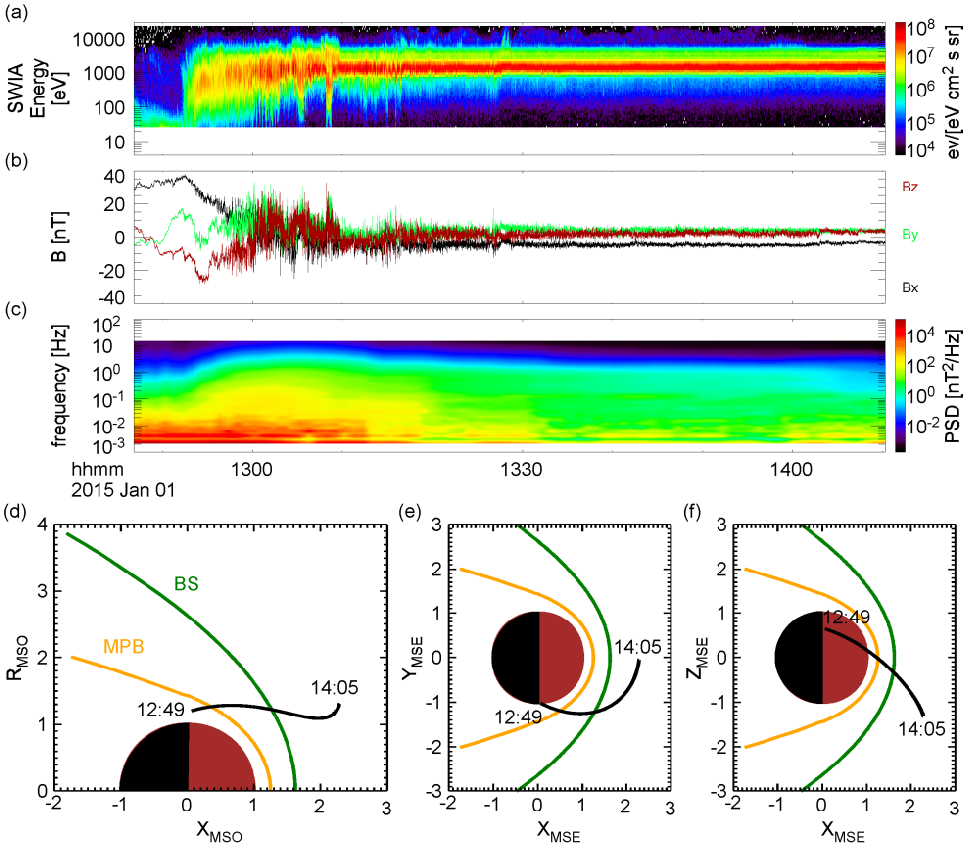

Figure 2. MAVEN observations and PSDs computed for magnetic field fluctuations for a portion of the MAVEN orbit. (a) The MAVEN Solar Wind Ion Analyzer (SWIA) measurements of the ion energy spectrum is shown here to merely give context for the observation. During this observation, the MAVEN spacecraft traversed from the magnetic pileup region which is typically populated by ions with energies < 100 eV, through the magnetosheath, which is populated by ions with energies centered at ~ 1 keV, and finally into the upstream region with ions that have energies centered also at 1 keV, but with a narrower temperature than in the magnetosheath. (b) Magnetic field time series. The magnetic field shows oscillations centered on various non-zero values because the spacecraft traversed through various regions of the Mars plasm environment during this time interval. As discussed in section 2, the solar wind magnetic field is subjected to compression and draping downstream of Mars' bow shock which lead to the variation of the local magnetic field. (c) Power spectral density for the magnetic field fluctuations computed using the wavelet transform. (d) The MAVEN orbit shown in a X_{MSO} vs $R_{MSO} = \sqrt{(Y_{MSO}^2 + Z_{MSO}^2)}$ map. (e) The MAVEN orbit in a X_{MSE} vs Y_{MSE} map. (f) The MAVEN orbit in a X_{MSE} vs Z_{MSE} map.

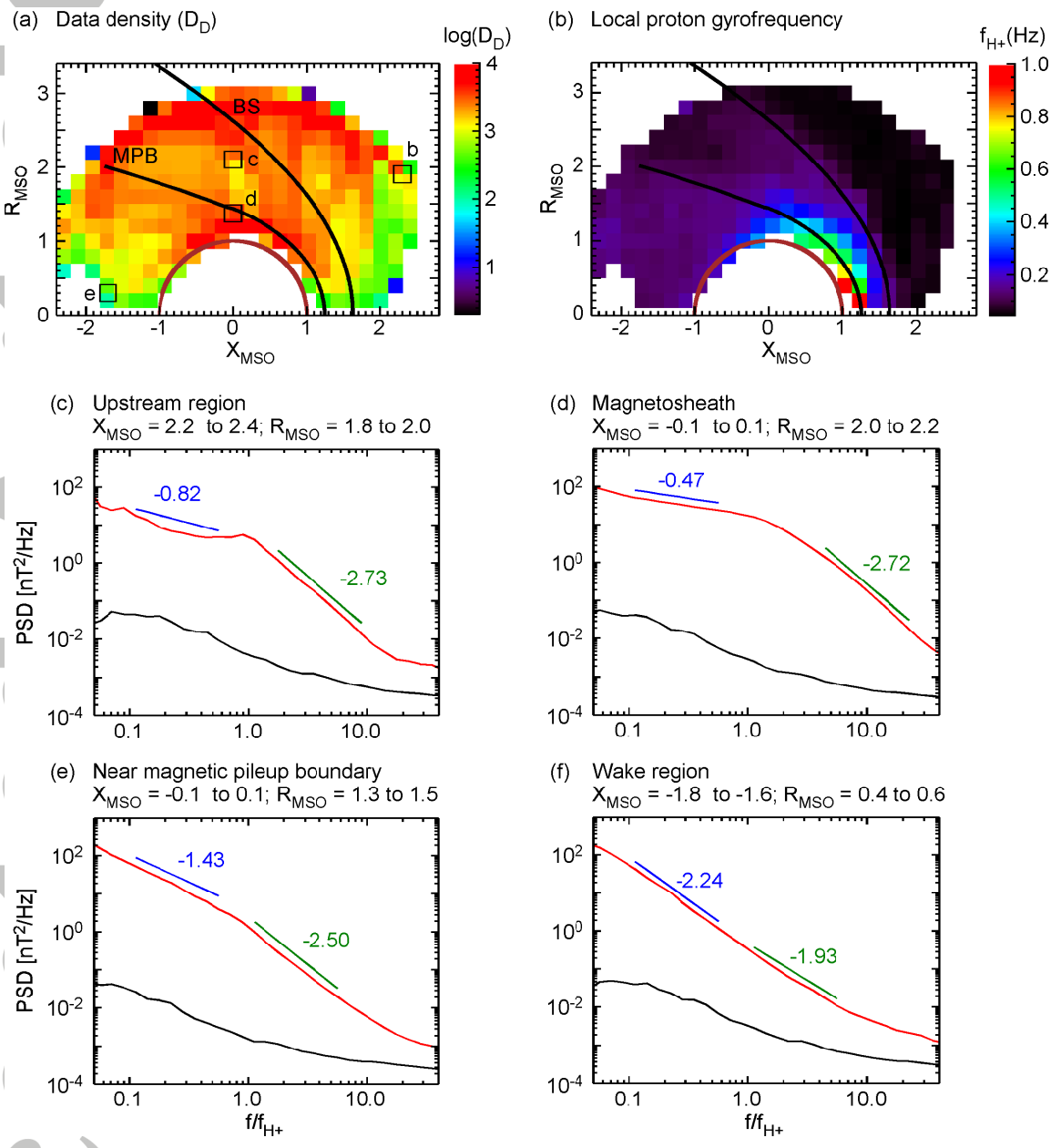

Figure 3. (a) MAVEN orbit coverage map showing data density D_D. (b) Median local proton gyrofrequency f_{H+}. (c)-(f) Median PSDs (shown in red) in four different regions of the Martian magnetosphere indicated in (a) by black squares. The black curves in (c) - (f) indicate the MAG noise level estimated by determining the minimum PSD for the magnetic field fluctuations measured by MAVEN when it was in the solar wind upstream of the bow shock. The spectral indices in the low- and high-frequency ranges (shown by a blue and a green line, respectively) have different values in different regions of the Martian magnetosphere.

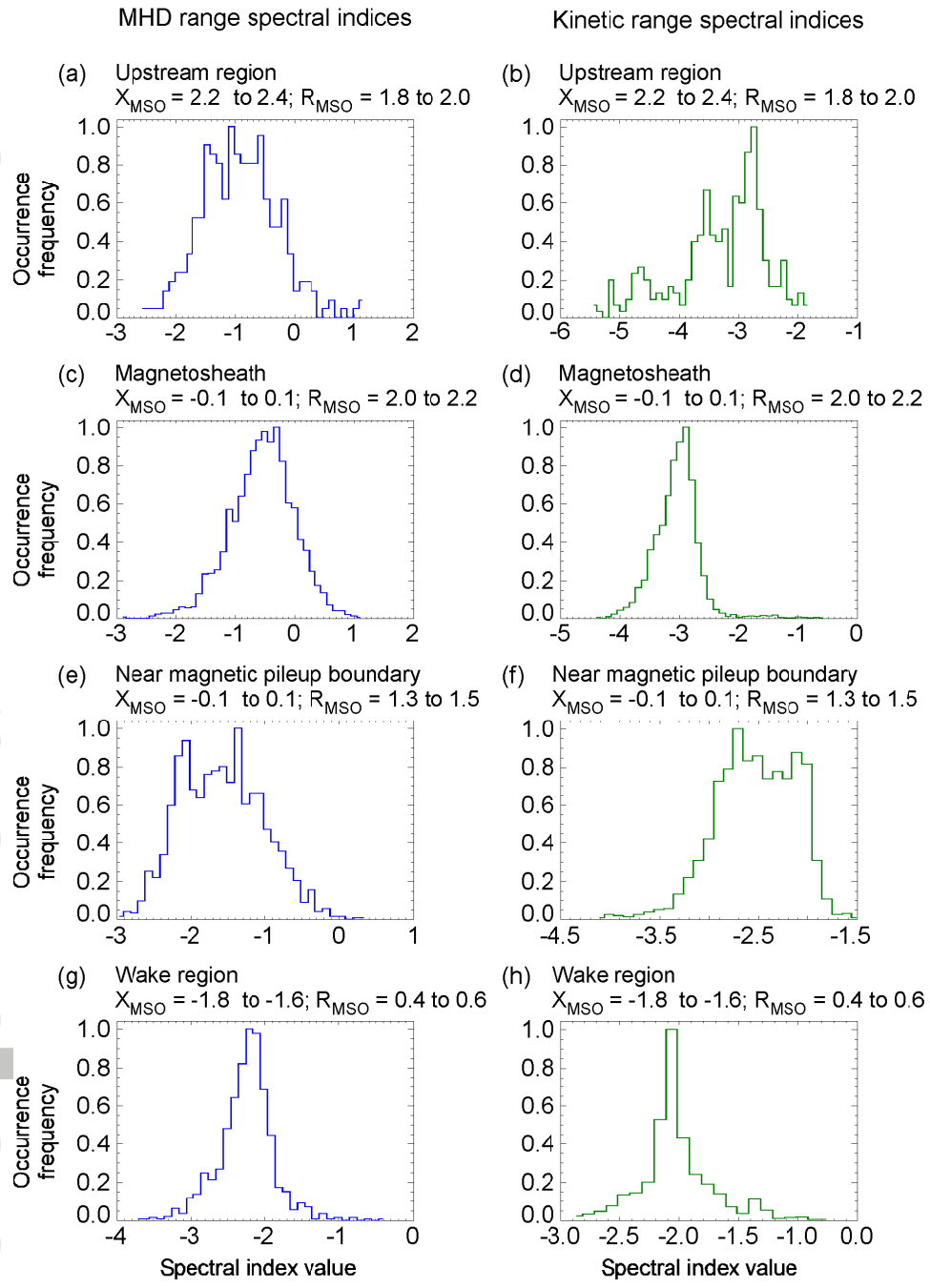

Figure 4. Histograms of spectral indices in the four different locations in the Mars plasma environment indicated in Figure 3(a). (a),(b) MHD and kinetic range spectral index histograms in the upstream region. (c),(d) MHD and kinetic range spectral index histograms in the magnetosheath. (e),(f) MHD and kinetic range spectral index histograms near the MPB. (g),(h) MHD and kinetic range spectral index histograms in the wake.

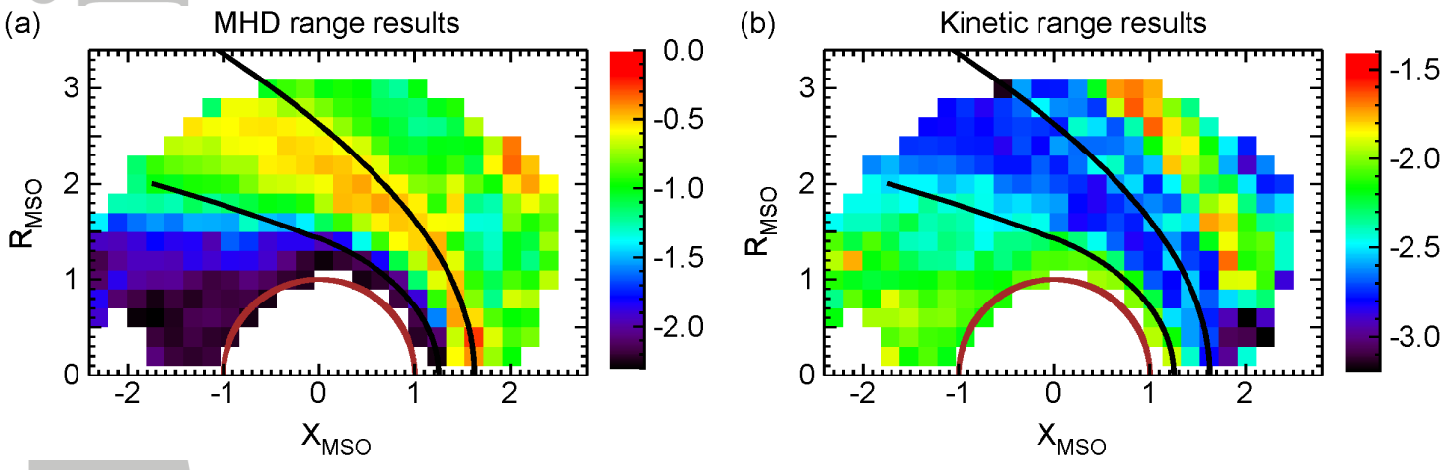

Figure 5. (a) MHD range spectral indices shown in a X_{MSO} vs $R_{MSO} = \sqrt{(Y_{MSO}^2 + Z_{MSO}^2)}$ map. (b) Kinetic range spectral indices shown in a X_{MSO} vs R_{MSO} map. The colors indicate the values of the spectral indices. The MHD range spectral index values decrease when going deeper into the magnetosphere. The kinetic range spectral indices show the opposite trend. The banded structure in the upstream region is a consequence of the fact that the spacecraft only covered apoapsis far out in the subsolar region in the $Ls \sim 270$ time range.

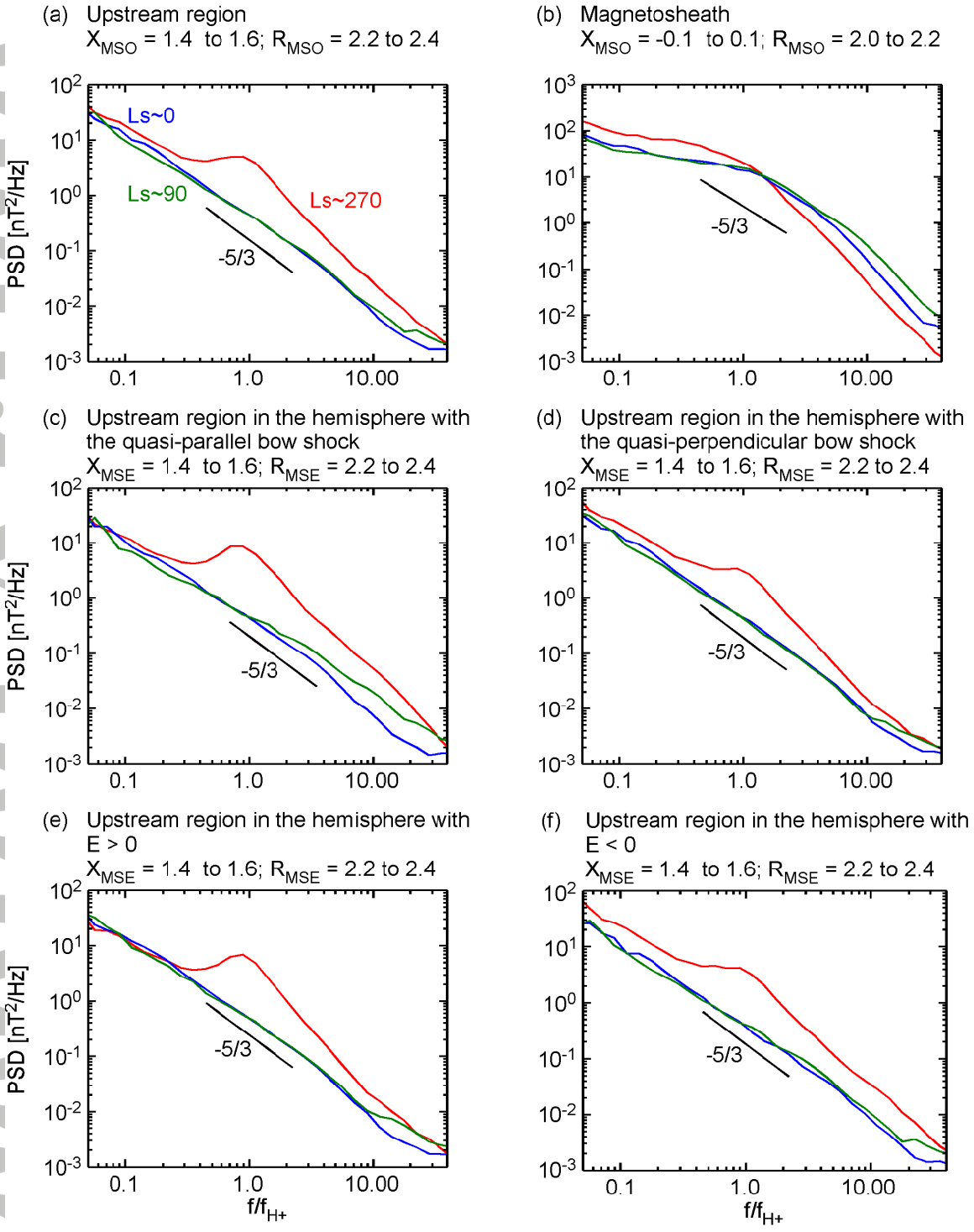

Figure 6. Power spectra for three seasons. (a)-(b) Power spectra in the upstream region and the magnetosheath. (c)-(d) Power spectra for the quasi-parallel and quasi-perpendicular regions. (e)-(f) Power spectra for the E> 0 and E< 0 regions. The black line depicts the slope corresponding to the Kolmogorov spectral index and it is shown here for reference.

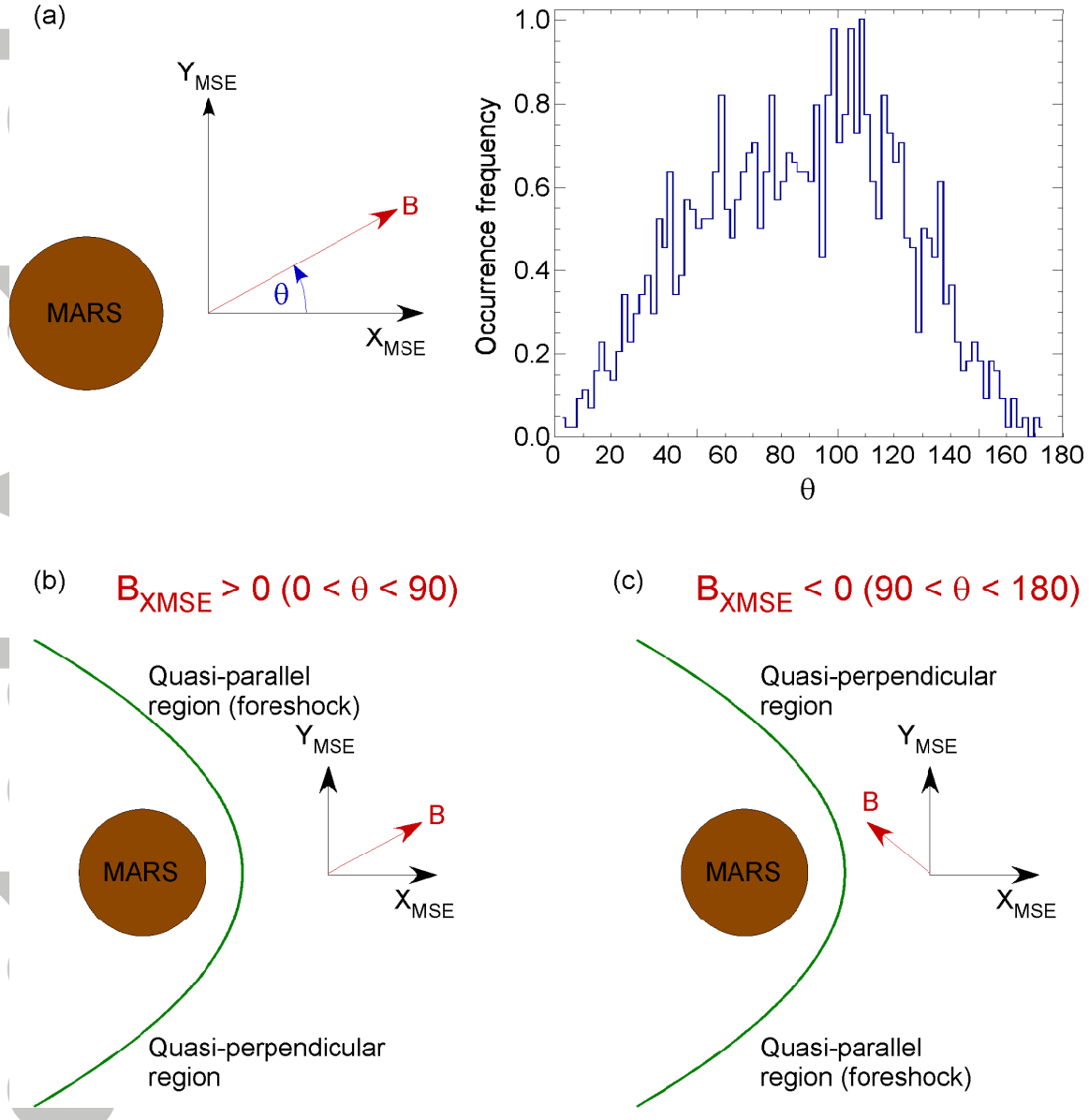

Figure 7. (a) Histogram of the upstream magnetic field orientation θ. The X_{MSE} direction is aligned opposite to the solar wind flow direction and the Y_{MSE} direction is aligned with the upstream magnetic field component perpendicular to the solar wind flow. Thus the sign of B_{XMSE} or the $X - MSE$ component of the magnetic field is indicative of the foreshock locations. (b) When $B_{XMSE} > 0$ or when $0^0 < \theta < 90^0$ the quasi-parallel shock or the foreshock region is located at $Y_{MSE} > 0$, whereas the quasi-perpendicular shock region is located at $Y_{MSE} < 0$. (c) When $B_{XMSE} < 0$ or when $90^0 < \theta < 180^0$ the quasi-parallel shock region is located at $Y_{MSE} < 0$, whereas the quasi-perpendicular shock region is located at $Y_{MSE} > 0$.

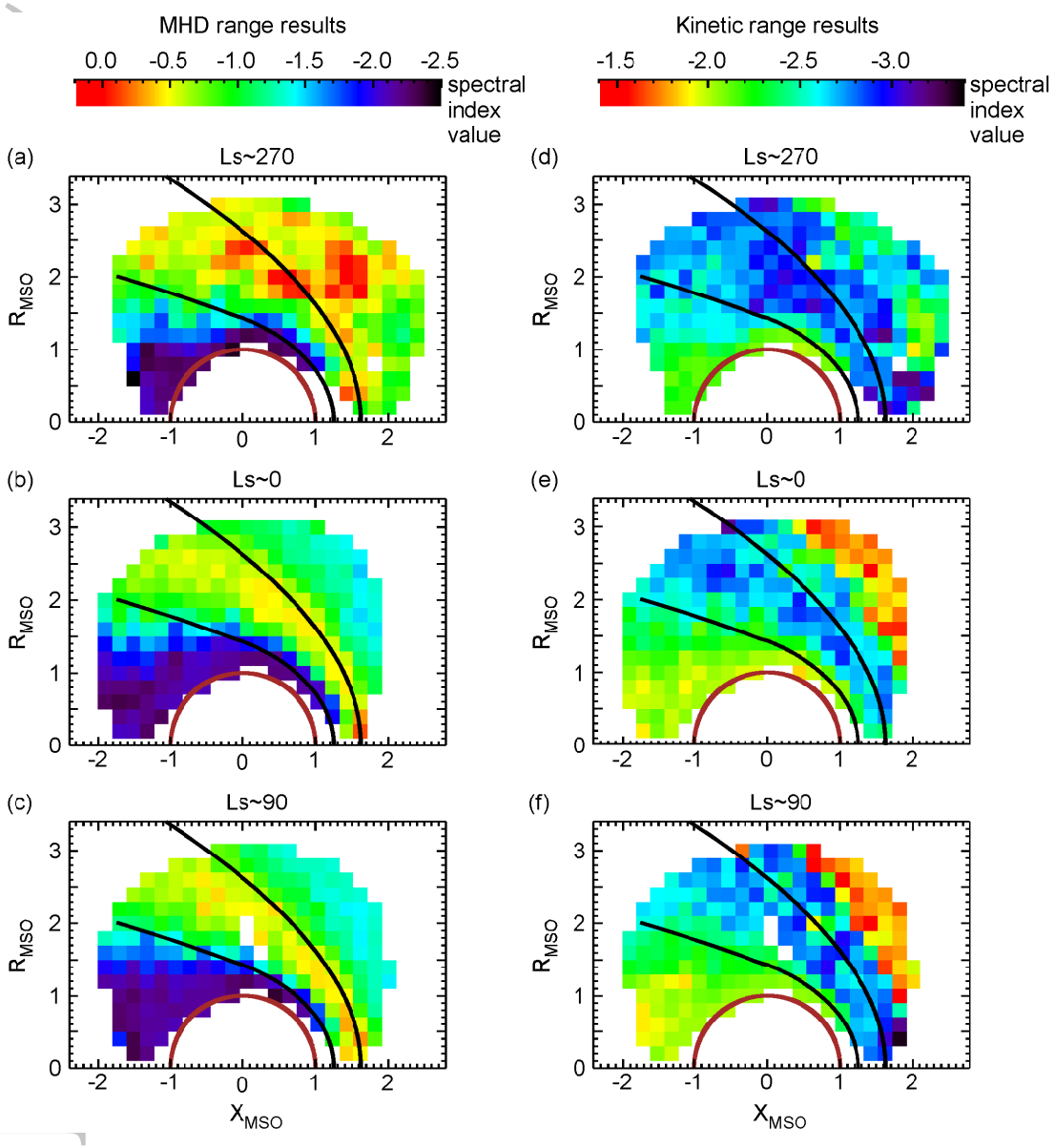

Figure 8. Seasonal variability of the spectral indices. (a)-(c) MSO orbit maps for the MHD range spectral indices for seasons Ls$\sim$ 270, Ls$\sim$ 0, and Ls$\sim$ 90. (d)-(f) MSO orbit maps for the kinetic range spectral indices for the same three seasons. The MHD range spectral indices show seasonal variability in the upstream region and in the magnetosheath while the kinetic range spectral indices show seasonal variability in the upstream region and in the night-side magnetic pileup region.

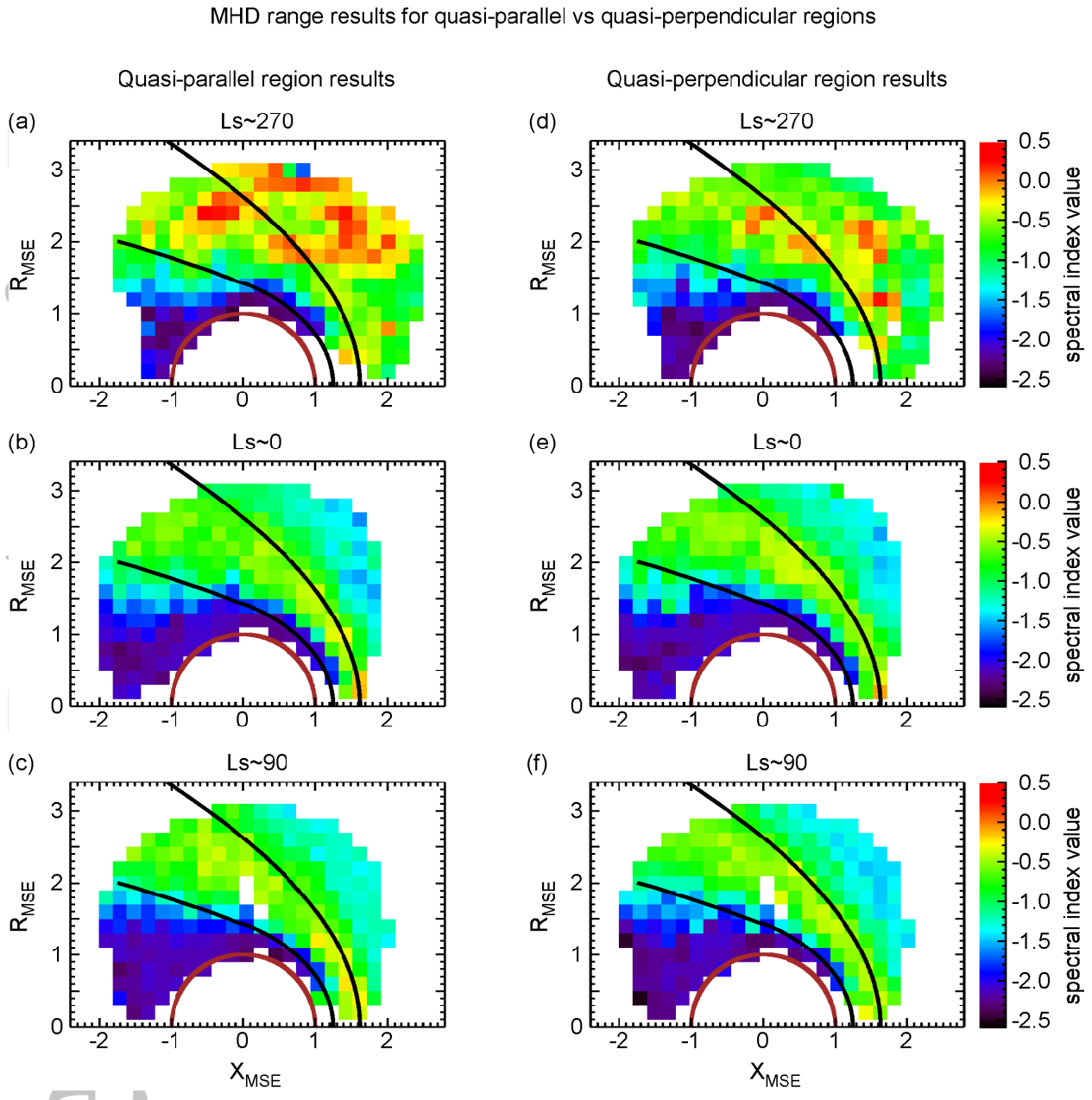

Figure 9. MHD range spectral indices in the magnetospheric hemispheres containing the quasi-parallel and the quasi-perpendicular shock regions. (a)-(c) Quasi-parallel region spectral indices plotted in X_{MSE} vs $R_{MSE} = \sqrt{(Y_{MSE}^2 + Z_{MSE}^2)}$ maps for the three seasons. (d)-(f) Quasi perpendicular region spectral indices plotted in X_{MSE} vs R_{MSE} maps. A prominent asymmetry for the spectral index values can be seen in the upstream region and in the magnetosheath for Ls∼270.

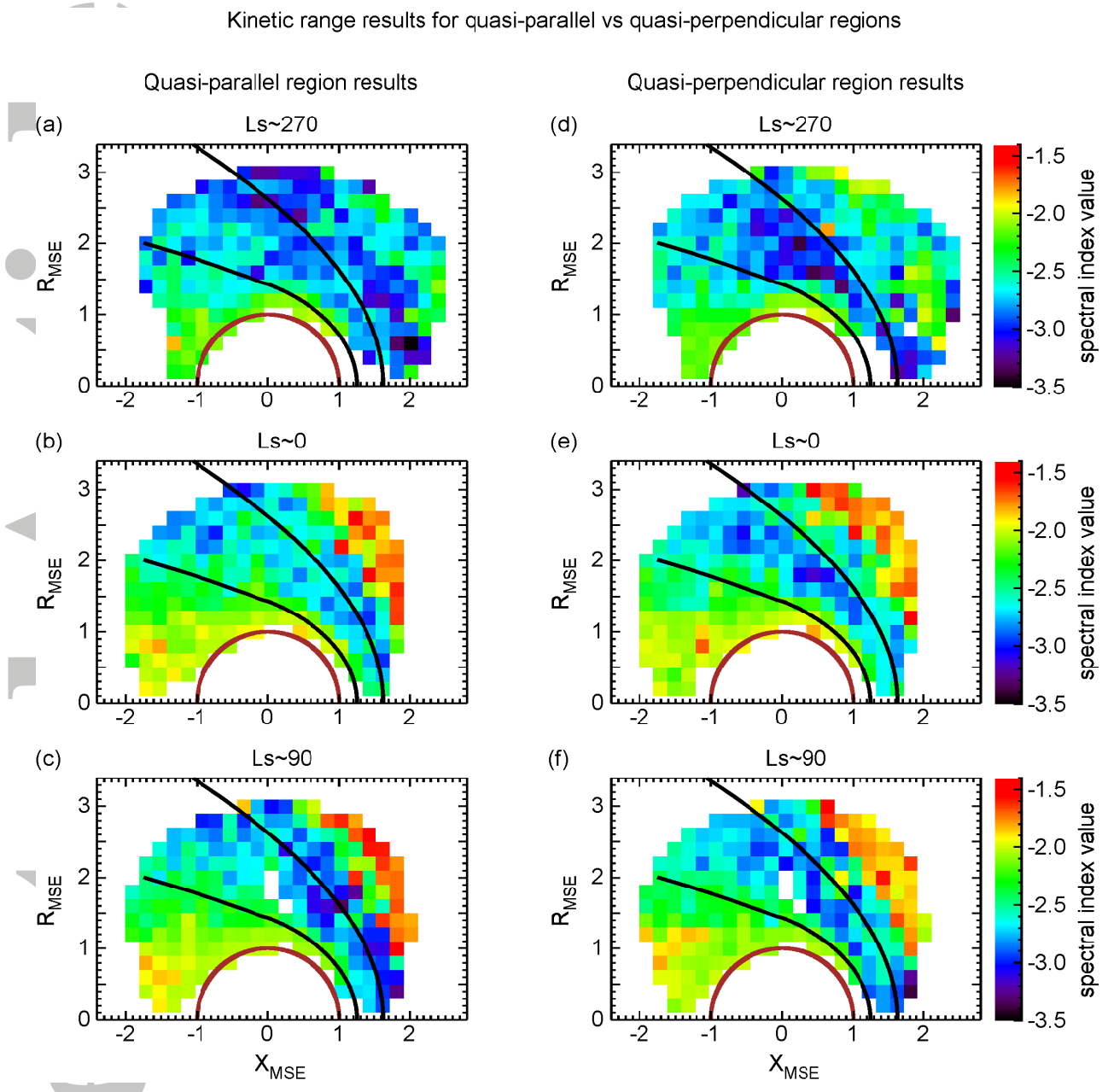

Figure 10. Kinetic range spectral indices in the magnetospheric hemispheres containing the quasi-parallel and quasi-perpendicular shock regions. (a)-(c) Quasi-parallel region spectral indices plotted in X_{MSE} vs R_{MSE} maps for the three seasons. (d)-(f) Quasi-perpendicular region spectral indices plotted in X_{MSE} vs R_{MSE} maps. An asymmetry is present for the spectral index values between the quasi-parallel and quasi-perpendicular regions for Ls∼270.

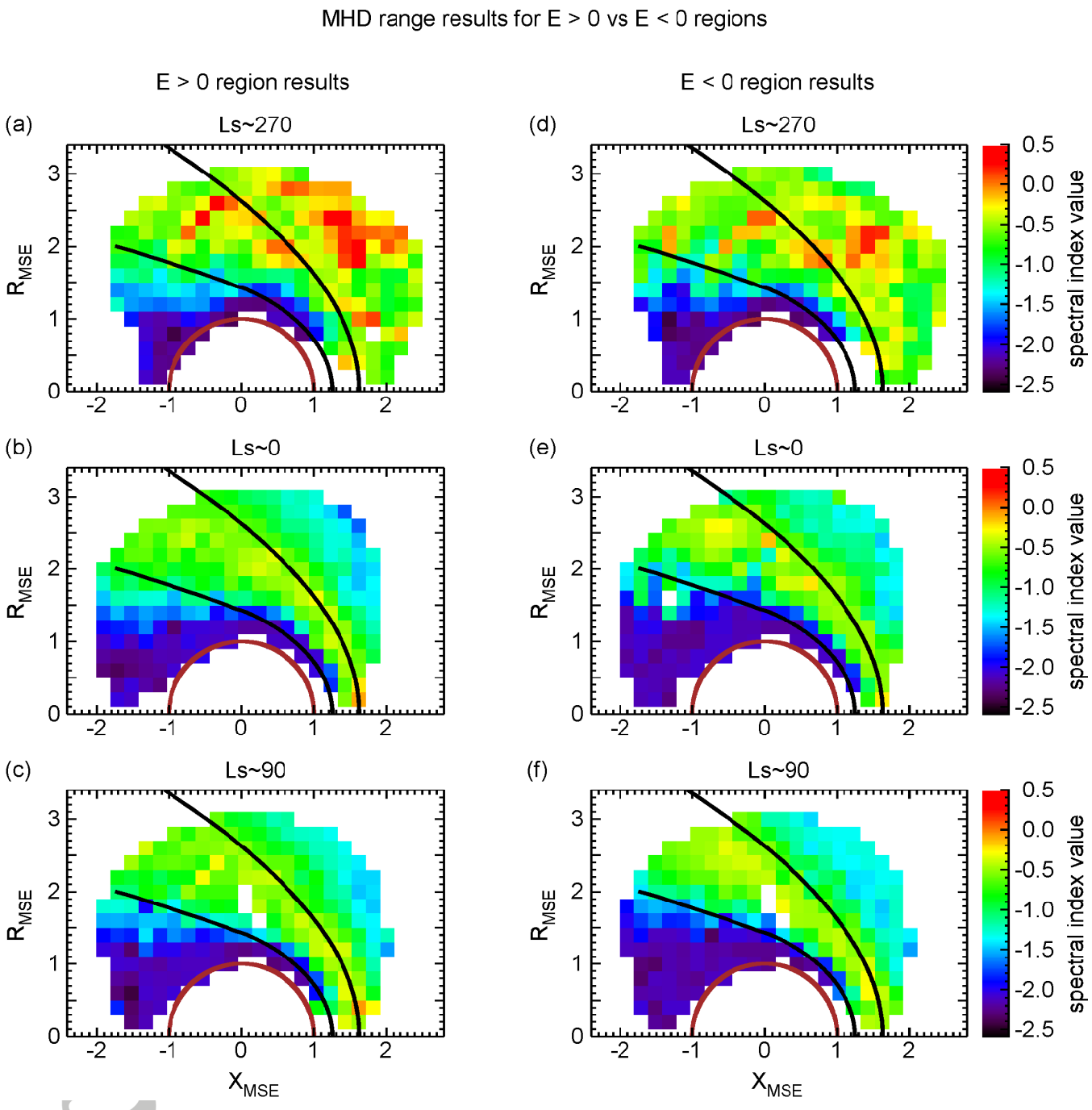

Figure 11. MHD range spectral indices in the magnetospheric hemispheres facing the positive and negative upstream electric field directions plotted in X_{MSE} vs R_{MSE} maps. (a)-(c) Orbit maps for the E > 0 region spectral indices. (d)-(f) Orbit maps for the E < 0 region spectral indices. The spectral indices show asymmetry in the upstream region for Ls∼270.

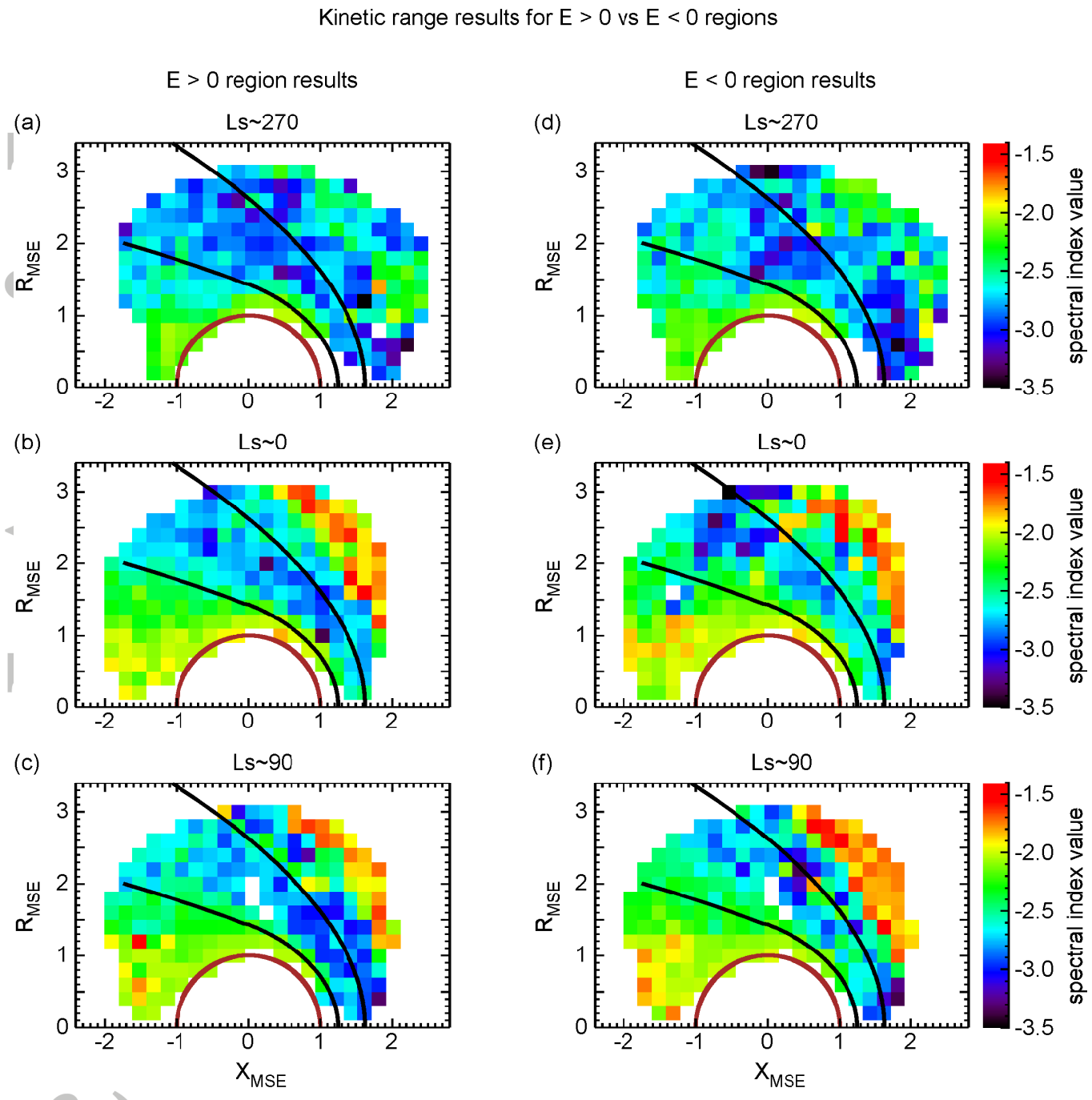

Figure 12. Kinetic range spectral indices in the magnetospheric hemispheres in the positive and negative electric field directions plotted in X_{MSE} vs R_{MSE} maps. (a)-(c) Orbit maps for the E > 0 region spectral indices. (d)-(f) Orbit maps for the E < 0 region spectral indices. The spectral indices do not show a discernible asymmetry in any of the seasons.